بسم الله الرحمن الرحيم

الجمهورية الجزائرية الديمقراطية الشعبية
REPUBLIQUE ALGERIENNE DEMOCRATIQUE ET POPULAIRE

MINISTERE DE L'ENSEIGNEMENT SUPERIEUR
et de la RECHERCHE SCIENTIFIQUE
UNIVERSITE SAAD DAHLAB – BLIDA 1

وزارة التعليم العالي والبحث العلمي
جامعة سعد دحلب - البليدة 1

Faculté des Sciences
Département de Physique

كلية العلوم
قسم الفيزياء

MEMOIRE

De fin d'étude en vue de l'obtention du diplôme de Master académique

Spécialité : Matière Rayonnements

Présenté par : **Kheireddine MAHDI**

Thème

Comparison between Firsov and Lindhard-Scharff-Schiott (LSS) stopping power models.

Soutenu Publiquement le : 11/09/2017 devant le jury composé de :

Mr. Mohamed SIDOUMOU	Maitre de conférence, USDB1	Président
Mr. Mamoune CHEKIRINE	Maitre de conférence, USDB1	Examinateur
Mr. Abdelkader GUESMIA	Maitre de conférence, USDB1	Directeur de thèse

Année universitaire 2016 / 2017

إهداء

إلى والدتي،

إلى والدي،

إلى إخوتي و أخواتي و أبنائهم،

إلى كل الذين عرفتهم، أو التقيتهم، أو سمعت عنهم، و تركوا بصمات طيبة في حياتي.

Abstract

This work presents a comparison between Firsov and the Lindhard-Scharff-Schiott (LSS) stopping power models and experimental data. Firstly the background and the results of the Thomas-Fermi model on which the Firsov and Lindhard-Sharff-Schiott (LSS) stopping power models are based are discussed before presenting the Firsov and LSS models and comparing between them. In a second time, the results of the stopping powers of some projectiles, obtained by using LSS model, Firsov's model, the SRIM program and available data, each one in 3 or 4 different targets are discussed, and we finish by discussing the Z oscillations which are due to the shell structure of the atoms.

ملخص

يعرض هذا العمل مقارنة بين نموذجي قدرة الإيقاف لكل من فيرسوف و لينهارد-شارف-سكيوت (لسس) والبيانات التجريبية. قمنا أولا بمناقشة فرضيات ونتائج النموذج الذري لتوماس-فيرمي الذي يستند إليه النموذجان سالفا الذكر قبل عرضهما و مقارنتهما. بعد ذلك ناقشنا حسب البيانات التجريبية المتاحة نتائج قدرة الإيقاف لبعض القذائف ، المتحصل عليها عن طريق نموذج لسس، و نموذج فيرسوف، و برنامج سريم، كل قذيفة في 3 أو 4 أهداف مختلفة. و أنهينا البحث بمناقشة التذبذبات الناتجة عن تغير الرقم الذري للهدف.

Acknowledgments

« First of all, I thank almighty God who gave me this chance and helped me in all aspects for the successful accomplishment of my study»

I would like to express my heartfelt gratitude to my advisor Dr Abdelkader GUESMIA for agreeing to be the sponsor of my memory and for his encouragement, help and the improvement of my scientific knowledge.

My thanks go also to Dr Mohammed SIDOUMOU for honoring me to preside over the memory jury.

I would like to thank Dr Mamoune CHEKIRIN for having accepted to participate in the jury and for his interest in this work.

I also express my gratitude to Dr L. BABA AHMED, Pr Mohamed El Amine BENAMAR and all the members of the "FUNDAPL" laboratory of the University of SAAD DAHLAB -BLIDA 1.

Contents

Chapter I

Introduction

In this chapter we present a general description of the slowing down of swift ions in matter, a historical review of the existing theories of the slowing down of swift ions in matter, the motivation of studying of the slowing down of swift heavy ions at low energies and frame the work in its scientific context.

1. General description of the slowing down of swift ions in matter:

Whenever an energetic charged particle, passes through a matter, it loses a certain fraction of its energy by collision with atoms of the stopper material. This loss depends on the stopper material nature, and energy of the incident ions.

Conceptually, for a quantitative understanding, the slowing down of energetic ions in matter is described by a fundamental parameter, S, alternatively called **stopping force** or **stopping power** or **linear energy transfer** (LET).

When an ion of energy E cross an infinitesimal thickness Δx in the matter, it losses some of its energy, ΔE, by collision with target atoms (See Fig. I.1).

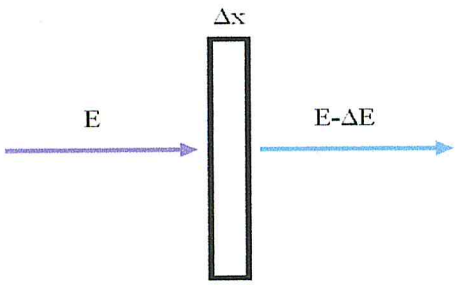

Fig. I.1: Energy loss of an ion after crossing matter

The mean of energy loss by path length is called the stopping power of this ion in this matter at the energy E:

$$S(E) = -\frac{1}{\rho}\frac{\Delta E}{\Delta x} \quad (\rho \text{ is the density of the target}) \qquad (I.1)$$

The stopping power has a force dimension, which is why it is also referred to as the stopping force[1] [Sig-2000]. Energy loss and linear energy transfer are used alternatively as well.

[1] Stopping power is an historical phrase, and Stopping Force would be more accurate.

The loss of energy results from various interaction processes such as:

1. Excitation and ionization of target electrons,
2. Projectile excitation and ionization,
3. Electron capture,
4. Recoil loss ('nuclear stopping'),
5. Electromagnetic radiation.

For light ions electromagnetic radiation (the 5th process) is negligible up to very high velocities and process 1 dominates except at very low-speed. But for heavier ions, the processes 2 and 3 cannot be neglected in general and, moreover, nuclear stopping becomes relatively more important at low and moderate velocities. Radiative processes become dominating at extremely high velocities [Sig-2004].

It is customary to distinguish two different mechanisms of energy loss:

1) Nuclear stopping power, in which energy is transmitted as translatory motion to a target atom as a whole.

2) Electronic stopping power, in which the moving particle loses its kinetic energy by exciting or ejecting atomic electrons.

For most purposes, this separation into elastic (nuclear) and inelastic (electronic) collisions is a convenient one [Nas-2015]. The energy-loss rate $\frac{dE}{dx}$ can thus be expressed as:

$$\frac{dE}{dx} = \left.\frac{dE}{dx}\right|_n + \left.\frac{dE}{dx}\right|_e$$

Where the subscripts n and e denote nuclear and electronic collisions, respectively.

In both cases, the interaction is basically of a Coulomb type; for the electronic case, it is pure Coulomb, while in the nuclear case, it is a form of screened Coulomb potential at low energy [Ter-2007].

Nuclear collisions can involve discrete energy losses and significant angular deflection of the trajectory of the ion. This process is responsible for the production of lattice disorder by the displacement of atoms from their positions in the lattice as well as direct backscattering events in Rutherford backscattering spectrometry. Electronic collisions involve negligible

deflection of the ion trajectory, and negligible lattice disorder [Nas-2015]. The relative importance of the two energy-loss mechanisms changes with the velocity and atomic number Z1 of the projectile. The nuclear stopping predominates for low velocity and high Z1, and electronic stopping predominates for high velocity and low Z1.

A comparison of the nuclear and electronic energy loss rates expressed is shown in Fig. I. 2.

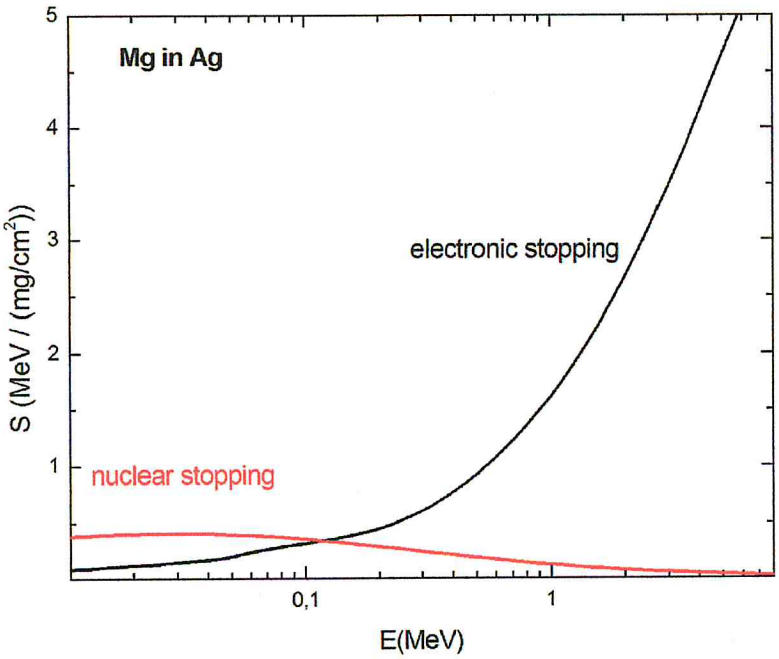

Fig. I. 2: Comparison between nuclear and electronic stopping power. The maximum of the nuclear stopping curve typically occurs at energies between 10-100 keV (Drawn by the program SRIM).

In this work only the electronic stopping power is concerned, so in the following we shall write stopping power and we don't have to specify that it is the electronic stopping power except when confusion is possible.

Another classification according to the ion energy is essential to highlight a physical model of energy loss (see Fig. I.). The low energies region (region I) contain the LSS (Lindhard, Sharff and Schiott) domain of energies where the stopping power is approximately proportional to the ion velocity i.e. the square root of the ion energy [Gue-2016]. In this work we try to explore the stopping power in the LSS domain. We distinguish also the intermediate region (region II) and the Bethe-Bloch region for high energies of ions (region III) [Nas-2015].

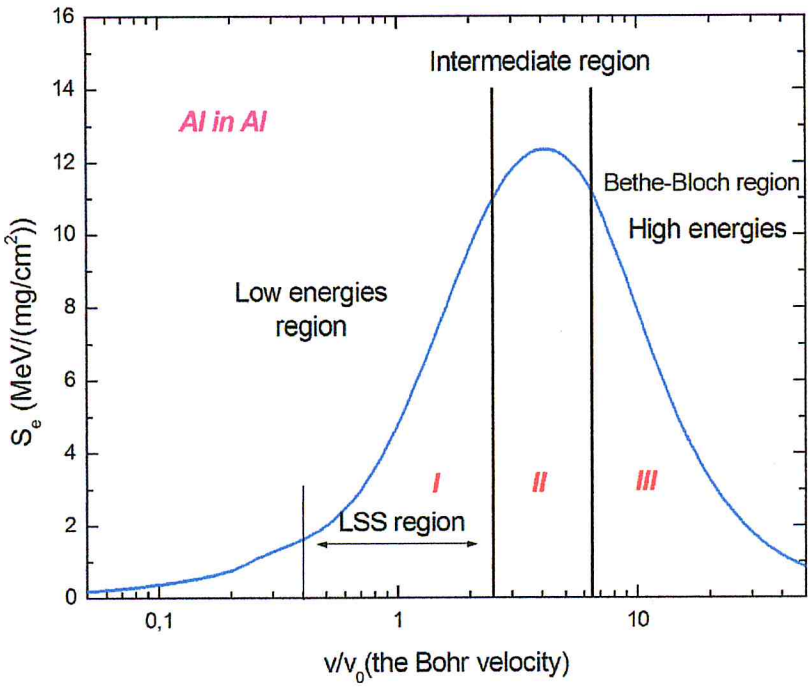

Fig. I.2: Electronic stopping power as a function of ion velocity and the LSS, intermediate and Bethe-Bloch regions.

2. Historical review:

The history of the penetration of a particle into matter might begin 400 years ago with the study of projectile ballistics, since the understanding of cannonballs in a viscous medium which is similar to the penetration of particles in matter [Zie-2008]. However, the subject of the stopping power and energy dissipation of charged particles through matter begin only the last century, from the discovery of radioactivity (in 1896 by Henri Becquerel while working with phosphorescent materials [All-1996]) which has offered well-defined beams with energies of several orders; before that, some experimental observations were made around 1850 in gas-discharge tubes, also the contribution of the identification of "cathode rays" and "canal rays" by Thomson in 1897 and Goldstein in 1902, and the observation of numerous phenomena [Sig-2006]. In 1900 Marie Curie is the first who speculates that alpha rays are material projectiles likely to lose their speed through the material. By changing the thickness of a metallic film she was able to find the energy loss of the alpha particles emitted from radium as a function of the density of the metal. Since such experiments have been carried out by scientists but these early studies were unable to create an energy deposition theory because there was not yet an accurate proposed model of the atom [Zie-2008].

The first theoretical treatment about scattering of electrically charged particles was published by J. J. Thomson in his classic book on electricity 'Conduction of electricity through gases', where he did not demonstrate the calculations of the energy loss in direct way, but he was interested in the problem of charged particle stopping [Hab-2011]. In 1911 Rutherford published his famous analysis leading to the structure of the atom as being made up of a heavy nucleus surrounded by electrons also this analysis established the concept of scattering cross section in order to describe statistically the interaction of fast particles with matter [Sig-2006].

These were the earlier studies in the domain, after that Niels Bohr and Hans Bethe proposed the first accurate and acceptable theories to study the energy deposition phenomena. In fact, they have succeeded in solving many limitations and problems corresponding to in the previous work carried out by Thomson and Darwin [Shu-2015].

In 1913 Bohr's classical approach for the electronic stopping power was unstable and served as a basis for the quantum mechanically description of the stopping problem. The discovery of the nuclear fission in 1938 [Hil-1989] gave the possibility for a detailed search on the penetration of high speed particles through matter [Kor-2006]. Bohr and Lindhard understood the difficulty and complexity of describing both the ion and the target particles during the collision. They connected the energy loss of fission ions along stopping path with the capture and loss of electrons by such particles [Boh-1954]. Bohr also recognized that the study of the stopping process is limited by knowledge of the ion charge state inside matter, which is estimated by the balance between electron capture and loss processes.

In the 1920s with the advent of quantum mechanics, Bohr's classical stopping model showed inconsistencies to explain the atomic phenomena because the transfer of energy occurs in discrete quantities. By using Bohr's approximation, Hans Bethe recreated the classical result in the quantum-mechanical treatment. The calculations in his new version are valid for relativistic energies.

Later Felix Bloch investigated the classical and quantum-mechanical approaches and found conditions in which these theories could be used. Bloch made corrections to Bethe's model and got the formula, which is valid for Bethe's result as well as for Bohr's [Kor-2006].

In 1958 Firsov used numerical techniques to derive the interatomic potentials of two colliding atoms treated by the Thomas-Fermi atomic model, then he adapted these potentials using the Thomas-Fermi screening length in order to get his stopping power formula for low velocities [Fir-1958-a,b]. Another important model for low velocities was the lindhard,

scharff and schiott theory (commonly called LSS theory) [Lin-1963]. LSS theory was the peak of stopping and range theory based on statistical atoms [Zie-2008]. In this work, we are interested in the tow last theories which will be well described in the next chapter.

3. Motivation:

The stopping power parameter is an indispensable and critical quantity in several fields of technology using the interaction of an ion beam with a target [Gue-2014]. Let us mention some of uses area:

3.1. Ion beam analytical techniques for surface and rear surface characterization:

Materials analysis by ion beams is developing day by day as a powerful tool based on a variety of physical mechanisms, for example:

- **The Rutherford Backscattering Spectrometry (RBS)** which is used to determine the structure and composition of materials by measuring the backscattering of a beam of ions,
- **The Particle-Induced X-ray Emission (PIXE)** which is used to determine the elemental composition of a sample, when it is exposed to an ion beam, its atomic interactions give rise to electromagnetic radiation of the wavelengths in the X-ray part of the electromagnetic spectrum.
- **Nuclear reaction analysis** (NRA) which is based on the study of gamma electromagnetic radiations or particles emitted during nuclear interactions between a beam of high-energy incident ions and the nuclei of the atoms of the target to be studied.

In all these analysis methods and others using ion beams, knowing the stopping power of the beam ions with good accuracy, is extremely necessary to get reliable results [Msi-2009].

3.2. Ion implantation:

It is used to implant the beam ions of one material into another solid, thereby changing the physical, chemical or electrical properties of target. In order to get good results, a well control of two important experimental parameters is extremely necessary: the beam intensity which determines the number of implanted ions and the beam energy which determines the

of two important experimental parameters is extremely necessary: the beam intensity which determines the number of implanted ions and the beam energy which determines the implant depth [Msi-2014]. It is clear that the second parameter has no sense without knowing the implanted ion range (including energy loss).

3.3. Radiation protection and radiation therapy:

Since the discovery radioactivity, undesired radiation effects on living tissue have been a major problem for radiation research. Radiation protection and dosimetry and the development of standards involve measurements with charged-particle beams at all stages, and highly advanced theoretical calculations enter here [Sig-2006].

Also in radiation therapy which is a type of cancer treatment that uses ion beams to destroy the tumor cells. The energy loss and ranges need to fore carefully studied before setting up the radiation treatment to maximize the damage for the tumor and minimize the potential damage to the healthy tissue.

Performing an experiment to determine the stopping power of a projectile at a well-defined energy using thin films is very expensive, and although many experimental data have been published for the last decades, many deficiencies and discrepancies appear in these data, thus they become often incapable of satisfying many needs of the different fields of applications [Gue-2015]. For example, in radiation therapy, tumor treatment with heavy ion beams exhibits several advantages, for example range straggling and lateral scattering are small [Lan-1996]. Therefore, an accurate theoretical expression of stopping power is extremely needed in order to fill the gaps in experimental data.

In this chapter, we have presented a general description of the slowing down of swift ions in matter and two ways to classify the stopping power according to the interaction processes and the ion energy, and then we have presented a historical review of the existing theories of the slowing down of swift ions in matter, and we have finish by introducing some applications of the stopping power parameter.

Chapter II

Fundamental Theories of the Stopping Power at Low Velocities

1. Introduction

In this chapter we begin by presenting the cross section concept and a general expression of the stopping power as a function of the cross section. A short discussion of the background of the Atomic Thomas-Fermi model on which the Firsov and Lindhard-Sharff-Schiott (LSS) stopping power models are based, will be doing. We present the Firsov and LSS models and a comparison between them, and we finish by discussing the widely used software package SRIM (Stopping and Range of Ions in Matter).

2. The cross section concept

The general theories of the stopping power are fundamentally based on the concept of transfer cross section.

A detailed description of the concept of cross section can be found in course of Interaction of ions with matter [GUE-2016]. The cross section is a fundamental concept in all theories of penetration of ions in matter. In order to understand easily the concept of the cross section we begin the simple case of collision of point projectile with a hard sphere of radius a (see Fig. II.1)

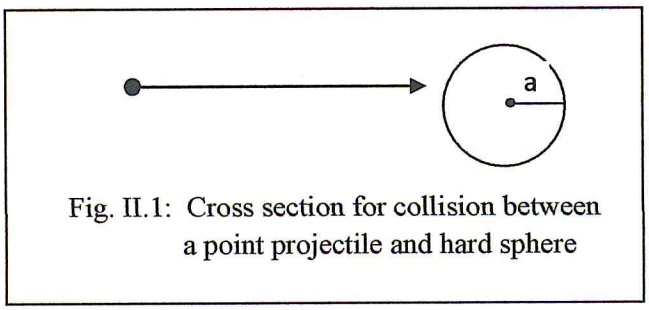

Fig. II.1: Cross section for collision between a point projectile and hard sphere

It is clear that, all incident point projectile which are in the area πa^2 make a collision with the target sphere, this cross area is called the collision cross section.

Microscopically, we have not a simple relationship between the cross section and the physical size of the particles. The magnitude of a given cross section depends on the target, the projectile, and their relative velocity, and also on the process that we want to watch it, for example ionization, excitation, nuclear reaction, emission of specific particles and so on [Sig-2006].

In order to define the cross-section, let some microscopic target of thickness Δx and atomic density N to be bombarded by a beam of projectiles of flux I spread homogeneously over an area A (Fig. II.2).

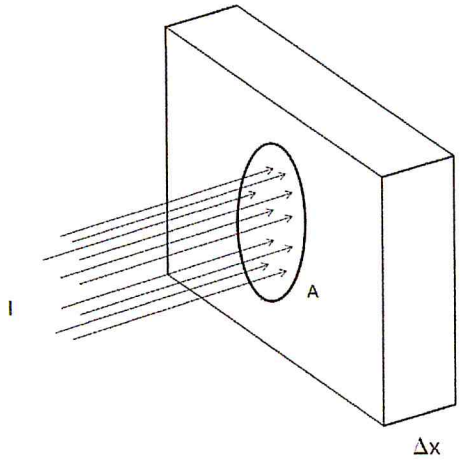

Fig. II.2: Macroscopic target bombarded by a beam.

We consider that the thickness Δx of the target is very small and the particles of the target are sufficiently distant from each other, so that an incident particle interacts almost with one target particle. We thus neglect the processes of multiple scattering. Let σ_i the cross section for some process i (excitation, ionization, scattered, recoiled ...). With this consideration, everything happens as if we have a surface A containing $N\Delta xA$ diffusing centers and these centers occupy an effective section equal to $\sigma_i N\Delta xA$. Thus, there is only one part of the surface A that interacts, so we can deduce the probability of interaction of the beam:

$$p_i = \frac{(N\Delta xA)\sigma_i}{A} = \frac{\text{the } effective\ area}{\text{the total area}} = N\Delta x\sigma_i \qquad \text{(II.1.a)}$$

Experimentally the last probability can be measured by the number, $N_{interact\,ii}$, of particles detected (interact: excite, scattered, recoiled...) over the space per unit time, divided by the number, $N_{incident}$, of incident ions by unit of time. The number $N_{interact\,ii}$ is equal to the product of the incident flux I (I is defined as the number of particles per unit time crossing a unit area normal to direction of incidence) by the area A.

$$p_i = \frac{N_{interact\,ii}}{IA} \qquad \text{(II.1.b)}$$

The comparison of Eqs. (II.1.a) and (II.1.b) gives the cross section for all interactions:

$$\sigma = \frac{N_{interact}}{IN\Delta xA} \qquad \text{(II.2)}$$

Note that for theoretical calculation of the total cross section the last equation is considered by taking the number of target particles $N\Delta xA$ equal to one, then the total cross section is given as:

$$\sigma = \frac{N_{interact}}{I} \tag{II.3}$$

3. General expression of the stopping power

Consider a very thin layer of thickness Δx in the matter in the sense that one incident ion can produce almost one particular energy transfer.

If N ions of energy E traverse one by one a thickness Δx in the matter or we realize N times the experiment of traversing of one ion in matter of thickness Δx, for each experiment j (j = 1, 2…) we have a number n_i^j of particular energy transfer T_i.

The process of particular transfer energy T_i induces a mean energy loss by traversing one ion is given by:

$$\langle \Delta E \rangle_i = \frac{1}{N} \sum_{j=1}^{N} n_i^j T_i = T_i \frac{\sum_{j=1}^{N} n_i^j}{N} \tag{II.4}$$

It is clear that $\sum_{j=1}^{N} n_i^j$ represent the number of particular transfer of energy T_i for N incident ions, where n_i^j can take only the values 0 or 1 (the probability of a particular energy transfer T_i is very small). So, from II.1.a, we can write:

$$\langle \Delta E \rangle_i = T_i N \Delta x \sigma_i \tag{II.5}$$

Where σ_i is the cross section for the specific particular energy transfer i.

For all particular transfer, the mean energy loss for one collision is given by:

$$\langle \Delta E \rangle = N \Delta x \sum_i T_i \sigma_i \tag{II.6}$$

The stopping power is then, given by:

$$\frac{1}{\rho} \frac{\langle \Delta E \rangle}{\Delta x} = \frac{1}{\rho} N \sum_i T_i \sigma_i \tag{II.7}$$

In the literature $S = \sum_i T_i \sigma_i$ is called stopping power parameter [Sig-2006]

4. Thomas-Fermi atomic model

The Thomas-Fermi model is a semi classical theory that describes the electronic structure of atoms. The development of the Thomas-Fermi model is based on the determination of an average potential V(r) acting on the atomic electrons with electron density $\rho(r)$. [Gal-1990]

4.1. The free electron gas

Before introducing the Thomas-Fermi model for the ground state of multielectron atoms, we start by recalling the results of the quantum study of a system constituted of N free electrons confined in a cube of side L, called Fermi electron gas.

The wave function of a free electron in a box is given by:

$$\psi_{n_x,n_y,n_z}(r) = \left(\frac{8}{L^3}\right)^{1/2} \sin(k_x x)\sin(k_y y)\sin(k_z z) \tag{II.8}$$

$$\text{where } k_x = \frac{n_x\pi}{L}, k_y = \frac{n_y\pi}{L}, k_z = \frac{n_z\pi}{L}, \qquad \text{with } n_x, n_y, n_z = 1,2\cdots \tag{II.9}$$

the energy E of one free electron is given:

$$E(\vec{k}) = \frac{\hbar^2}{2m}({k_x}^2 + {k_y}^2 + {k_z}^2) = \frac{\hbar^2 k^2}{2m} \tag{II.10}$$

The vector $\vec{k} = k_x\vec{e_x} + k_y\vec{e_y} + k_z\vec{e_z}$ is called the wave vector.

From the boundary condition (II.9) each volume of $\frac{\pi^3}{L^3}$ in k-space contains one state, then the number of possible state containing in a sphere of radius k in space is equal to:

$$N_S = 2 \times \frac{1}{8}\frac{\frac{4\pi k^3}{3}}{\frac{\pi^3}{L^3}} = \frac{k^3}{3\pi^2}V \tag{II.11}$$

The factor 1/8 in the expression II.11 appears because k_x, k_y and k_z are positives and the factor 2 describe the two spin directions.

The substitution of Eq. (II.10) in Eq. (II.11) gives:

$$N_s = \frac{1}{3\pi^2}\left(\frac{2m}{\hbar^2}\right)^{3/2} V E^{3/2} \tag{II.12}$$

The density of states $D(E)$ describes the number of electron quantum states per unit of energy, and $D(E)$ d E represents the number of electron states inside the interval of energy $[E, E + dE]$. Thus, the density of states $D(E)$ is obtained by deriving $N_s(E)$:

$$D(E) = \frac{dN_s}{dE} = \frac{1}{2\pi^2}\left(\frac{2m}{\hbar^2}\right)^{3/2} V E^{1/2} \qquad \text{(II.13)}$$

At absolute zero temperature, it is well know that all the states are occupied up to the Fermi energy E_F, so the number N of electrons is given by:

$$N = \int_0^{E_F} D(E)\, dE = \frac{1}{3\pi^2}\left(\frac{2m}{\hbar^2}\right)^{3/2} V {E_F}^{3/2} \qquad \text{(II.14)}$$

Then, the Fermi energy is given by:

$$E_F = \frac{\hbar^2}{2m}(3\pi^2\rho)^{2/3} \qquad \text{(II.15)}$$

where ρ is the electronic density ($\rho = \frac{N}{V}$).

The electron velocity corresponding to the Fermi energy is called the Fermi velocity v_F where

$$v_F = \sqrt{\frac{2E_F}{m}} = \frac{\hbar}{m}(3\pi^2\rho)^{1/3} \qquad \text{(II.16)}$$

The wave vector corresponding to E_F is $\mathbf{k_F}$ (the Fermi wave vector), from (II.11) and (II.15) we deduce:

$$k_F = \frac{\sqrt{2mE_F}}{\hbar} = (3\pi^2\rho)^{1/3} \qquad \text{(II.17)}$$

If we suppose that $E = \frac{1}{2}mv^2$ we deduce from (II.13) the density of state as a function of the velocity v

$$D(v) = \sqrt{\frac{m}{2}}\frac{1}{2\pi^2}\left(\frac{2m}{\hbar^2}\right)^{3/2} V\, v \qquad \text{(II.18)}$$

The mean value of the electron velocity $\langle v_e \rangle$ is obtained by using (II.17) where

$$\langle v_e \rangle = \frac{\int_0^{v_F} vD(v)dv}{\int_0^{v_F} D(v)dv}$$

We get after inserting the v_F formula (equation (II.16))

$$\langle v_e \rangle = \frac{3}{4}\frac{\hbar}{m}(3\pi^2\rho)^{1/3} \qquad \text{(II.19)}$$

Noting that the total energy of a Fermi electron gas in the ground state is obtained by the integral

$$E_{tot} = \int_0^{E_F} ED(E)dE = \frac{3}{5}NE_F \qquad \text{(II.20)}$$

4.2. The Thomas-Fermi atomic model

Consider an atom of N electrons, the potential $\varphi(r)$ acting on one electron is generated by the nucleus and the other electrons. The Thomas-Fermi treatment of the atom consists to suppose that the variation of the potential $\varphi(r)$ is very slow. According to Merzbacher [Mer-1961] this later condition is verified if the potential verify the following condition:

$$\frac{1}{\varphi(r)}\frac{d\varphi(r)}{dr} << \frac{1}{\lambda(r)} \tag{II.20}$$

where the $\lambda(r)$ is the de Broglie associated associate wavelength to the electron at the position r. the eq (II.20) indicate that the potential $\varphi(r)$ must be practically constant over a distance of wavelength $\lambda(r)$ range. Then over a distance of wavelength range each electron can be considered as an electro of the Fermi gas of energy $\frac{p^2}{2m} - e\varphi(r)$.

The allowed energies of an electron can be written as:

$$E = E_i - e\varphi(r)$$

Where E_i is one allowed level of the Fermi gas.

If an electron is at the edge of the Fermi Sea, its momentum is $\boldsymbol{p}_F$ so that its total energy is.

$$E_{max} = E_F - e\varphi(r) \tag{II.21}$$

The maximum energy must be the same throughout the atom; otherwise the electrons will move to decrease their total energy, it means that E_F must be now a function of r.

Using (II.15) and (II.21) we get:

$$\rho(r) = \frac{1}{3\pi^2}\left(\frac{2m}{\hbar^2}\right)^{\frac{3}{2}}(E_{max} + e\varphi(r))^{3/2} \tag{II.22}$$

We denote by

$$e\Phi(r) = E_{max} + e\varphi(r) \tag{II.23}$$

So that the previous equation will be

$$\rho(r) = \frac{1}{3\pi^2}\left(\frac{2m}{\hbar^2}\right)^{\frac{3}{2}}(e\Phi(r))^{\frac{3}{2}} \; for\; \Phi \geq 0 \tag{II.24}$$

No electron is confined for $\Phi < 0$, consequently,

$$\rho = 0 \; for \; \phi < 0 \tag{II.25}$$

We consider the charge density $-e\rho(r)$ of electron as continuous, so that we can use the Poisson's equation of electrostatics to write

$$\Delta\phi(\mathbf{r}) = \frac{1}{r^2}\frac{d}{dr}\left(r^2\frac{d\phi(r)}{dr}\right) = \frac{e}{\varepsilon_0}\rho(r) \tag{II.26}$$

By inserting (II.24) in (II.26) we obtain

$$\frac{1}{r^2}\frac{d}{dr}\left(r^2\frac{d\phi(r)}{dr}\right)=\frac{e}{3\pi^2\varepsilon_0}\left(\frac{2m}{\hbar^2}\right)^{\frac{3}{2}}\left(e\phi(r)\right)^{\frac{3}{2}} \tag{II.27}$$

Also we get from (II.25) and (II.26)

$$\frac{1}{r^2}\frac{d}{dr}\left(r^2\frac{d\phi(r)}{dr}\right)=0 \quad for\ \phi<0 \tag{II.28}$$

when approaching the nucleus (i.e. $r\to 0$), the potential $\phi(r)$approaches $\frac{1}{4\pi\varepsilon_0}\frac{Ze^2}{r}$ (electrostatic potential of point charge) consequently

$$\lim_{r\to 0}\phi(r)=\frac{1}{4\pi\varepsilon_0}\frac{Ze^2}{r} \tag{II.29}$$

Let us put

$$\phi(r)=\frac{1}{4\pi\varepsilon_0}\frac{Ze}{r}\chi \tag{II.30}$$

So,

$$\frac{d\phi(r)}{dr}=\frac{Ze}{4\pi\varepsilon_0}\left[-\frac{1}{r^2}\chi+\frac{d\chi}{dr}\right]$$

Then it follows that

$$\frac{d}{dr}\left(r^2\frac{d\phi(r)}{dr}\right)=\frac{Ze}{4\pi\varepsilon_0}r\frac{d^2\chi}{dr^2} \tag{II.31}$$

By setting $r=bx$ where x is a dimensionless variable, (II.27) take the new form

$$\frac{d^2\chi}{dx^2}=\frac{2^{7/2}}{3\pi}\frac{1}{{a_0}^{3/2}}Z^{1/2}\frac{b\sqrt{b}}{x^{1/2}}\chi^{3/2} \tag{II.32}$$

where $a_0=4\pi\varepsilon_0\frac{\hbar^2}{me^2}$ is the Bohr radius.

we put

$$b\sqrt{b}=\frac{3\pi}{2^{7/2}}{a_0}^{3/2}Z^{-1/2} \tag{II.33}$$

It follows that

$$b=\frac{(3\pi)^{2/3}}{2^{7/3}}\frac{a_0}{Z^{1/3}} \tag{II.34}$$

$$b=\frac{1}{Z^{1/3}}0.885a_0 \tag{II.35}$$

It is clear from (II.35) that b has the dimension of length. So (II.32) is simplified to

$$\frac{d^2\chi}{dx^2}=\frac{\chi^{3/2}}{x^{1/2}} \quad for \quad \chi\geq 0 \tag{II.36}$$

This equation is known as the Thomas-Fermi equation. We deduce from (II.28) and (II.31) that $\frac{d^2\chi}{dr^2} = 0$ for $\chi < 0$. Thus the Thomas-Fermi equation becomes:

$$\frac{d^2\chi}{dx^2} = \frac{\chi^{3/2}}{x^{1/2}} \quad for \quad \chi \geq 0 \tag{II.37.a}$$

$$\frac{d^2\chi}{dx^2} = 0 \quad for \quad \chi < 0 \tag{II.37.b}$$

We get for the boundary condition at $r = 0$ from (II.29) and (II.30)

$$\chi(x) = 1 \quad at \quad x = 0 \tag{II.38}$$

It is clear that the potential vanishes when $r \to \infty$ that means

$$\lim_{r\to\infty} \phi(r) = 0 \tag{II.39}$$

So that we get the second boundary condition for the T-F equation

$$\chi(x) = 0 \quad at \quad x = \infty \tag{II.40}$$

The solution of equation in (II.37.b) is $C(x - x_0)$ where C is negative constant, and we must have

$$C = \chi'(x_0) \tag{II.41}$$

It means that $\chi(x)$ has one zero at most in the interval $(0, +\infty)$ and χ is positive in the interval $(0, x_0)$ and negative in $(x_0, +\infty)$.

The number of electron in the atom is obtained by integrating $\rho(r)$ in the space

$$4\pi \int_0^\infty \rho(r) r^2 dr = N \tag{II.42}$$

By using (II.24) and (II.34) equation (II.42) becomes

$$N = Z \int_0^{x_0} \sqrt{x}\chi(x)^{3/2} dx \tag{II.43}$$

By inserting (II.37.a) in (II.43) it becomes

$$N = Z \int_0^{x_0} x \frac{d^2\chi}{dx^2} dx$$

$$N = Z[x\frac{d\chi}{dx} - \chi]_0^{x_0}$$

$$x_0\chi'(x_0) = \frac{N-Z}{Z} \tag{II.44}$$

We consider first a neutral atom i.e. $N = Z$, so the derivative χ' vanishes at the same point as χ, therefore the point x_0 must be at infinity. Thus the graph of the numerical solution for neutral atom is given by:

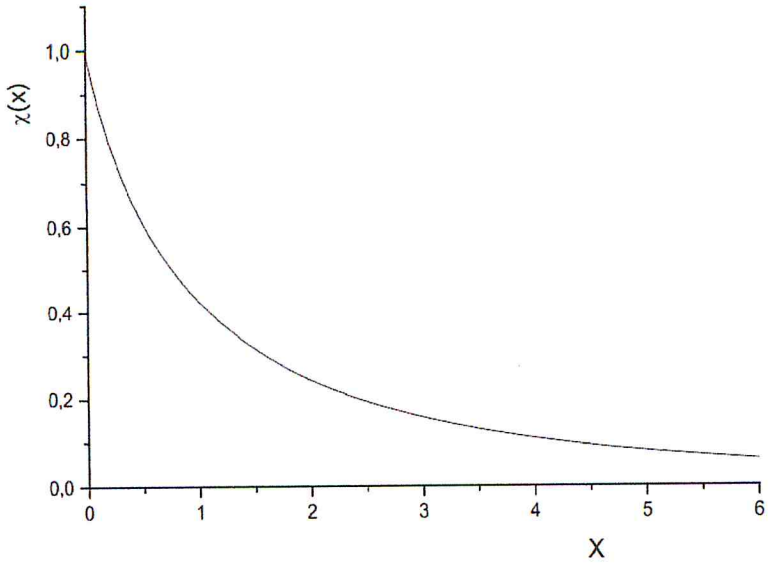

Fig. II.3: Graph of $\chi(x)$ for neutral atoms

Since $\chi(x)$ is known, we can deduce the potential energy (II.30)

$$\phi(r) = -\frac{1}{4\pi\varepsilon_0}\frac{Ze^2}{r}\chi \qquad \text{(II.45)}$$

For the case of ions, i.e. $N \neq Z$, we remark from equation (II.41) that $x_0\chi'(x_0) < 0$, so according to (II.42) we must have $N < Z$,thus we conclude that the T-F model cannot be applied to negative ions [Gal-1990].

5. Firsov Stopping power model

Consider an ion of low velocity v ($v < Z_1^{\frac{2}{3}}v_0$)[1], energy E, chargeZ_1, and mass m_1 collide an atom of mass m_2 at rest with impact parameter p_0. According to the Firsov's picture [Fir-1959] the transfer of energy ΔE, from the ion to the atom is due to the exchange of electrons between particles. The electrons pull out from the ion have the speed v of the ion; take place on the atom at higher energy levels. This exchange leads to an excitation of the target atoms by receiving energetic electrons and giving up slow electron to the ion. Thus the momentum of the ion decreases due to this process of interaction. The treatment of the momentum exchange between the incident ion and the atom electrons is subject to the following perceptions and approximations:

1. The motion and the distribution of electrons for both ion and atom are describing by the Thomas-Fermi model of the atom.

2. There is a minimum of the T-F potential on the surface joining the two particles (the superposition of the two T-F potential of the two atoms), this "Firsov's surface" S is perpendicular to the equipotential surfaces containing the minimum potential point. Thus the normal component of the electric field vanishes everywhere at the surface S.

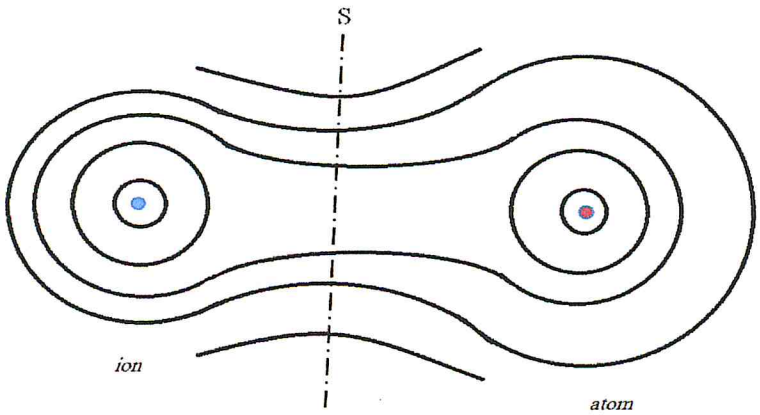

Fig. II.4: sketch of the equipotential surfaces during approaching of the ion and atom. Note that near the two nuclei the equipotential surfaces are spheres.

3. By using the Gauss theorem in case of a neutral quasimolecule (constitute by the two atoms: case treated by Firsov in his paper which consider the collision of two atom not ion-atom), the mean value of the electronic charge present in one side of the surface S is equal to the mean value of the charge of the corresponding nucleus [Fir-1959]. That is the reason why S divides the regions of the action of each atom during the collision. We can say that the Firsov's picture of the collision allow us the separation of the two teams (particle with its electrons) during any instant of the collision.
4. If electrons pass through the Firsov's surface, they interact strongly with the potential of the corresponding atom and lose their momentums which correspond on the average to the velocity of the ion.

The random electron flux across surface S in one direction r from the atom center is given (according to Maxwell distribution) by

$$\Gamma_S = \int d^3\vec{v}\, f(\vec{v},\vec{r},t)\vec{v}.\vec{u} = \frac{\rho(r)\langle v_e(r)\rangle}{4} \qquad \text{(II.47)}$$

where $\vec{u}$ is the unit vector normal to the surface S, f velocity distribution function, $\langle v_e(r)\rangle$ is the mean value of the electron velocity related to the electron density $\rho(r)$ according to the T-F model (equation (II.18)) by the following relation:

$$\langle v_e(r)\rangle = \frac{3}{4m}(3\pi^2)^{1/3}\hbar(\rho(r))^{1/3} \qquad \text{(II.48)}$$

where m is the electron mass. The force acting on the ion will be given by the expression

$$\vec{F} = m\frac{\overrightarrow{dR}}{dt} \underbrace{\int \frac{\rho(r)\langle v_e(r)\rangle}{4} dS}_{number\ of\ e^-\ traversing\ S\ by\ second} \quad \text{(II.49)}$$

where $\frac{d\vec{R}}{dt}$ is the velocity of the ion relatively to the atom.

The total work of slowing down of the ion is:

$$T = m\int \frac{dR}{dt} dR[\int \frac{\rho(r)\langle v_e(r)\rangle}{4} dS]$$

By using equation (II.49) we obtain

$$T = \frac{3}{16}(3\pi^2)^{1/3}\hbar \int\int \frac{dR}{dt} dR\,[\int (\rho(r))^{\frac{4}{3}} ds] \quad \text{(II.50)}$$

By inserting equation (II.24) which relies the potential ϕ and the electron density ρ, in equation (II.50) we get

$$T = \frac{m^2e^2}{4\pi^2\hbar^3}\int \frac{dR}{dt} dR[\int \phi^2 ds] \quad \text{(II.51)}$$

To perform the calculation of the energy lost in a single collision at impact parameter p the following additional assumption were made:

1. The loss of kinetic energy is small, thus we assume that the velocity of the projectile does not change during the collision so the relative motion of collisions partners was taken as rectilinear and uniform

$$\| \frac{d\vec{R}}{dt} \| = v \quad \text{(II.52)}$$

2. The Firsov's surface is considered plane perpendicular and placed on the midway of the segment joining the tow nuclei, as it is showed in Fig. II.5.

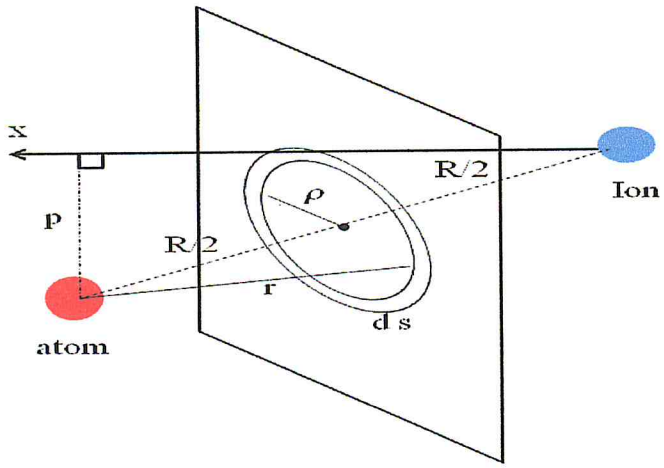

Fig. II.5: Geometry consideration Firsov's calculation

With these considerations we can write:

$$\frac{\overrightarrow{dR}}{dt}\overrightarrow{dR} = \frac{\overrightarrow{dR}}{dt}dR_{\parallel} = vdx \qquad \text{(II.53)}$$

By inserting (II.53) in (II.51) we get

$$T = \frac{m^2e^2}{4\pi^2\hbar^3}\int_{-\infty}^{+\infty}[\int \phi^2 ds]dx$$

In addition to all considerations, Firsov choose the potential $\phi(r)$ in the space between atoms as given by the expression of interaction potential of atom [Fir 1958-a]:

$$\phi(r) = \frac{Z_1Z_2}{r}\chi(1.13(Z_1+Z_2)^{\frac{1}{3}}\frac{r}{a_0}) \qquad \text{(II.54)}$$

Where χ is the universal T-F screening function where r is expressed in atomic unit($1a.u = a_0 = 0.529$ Å).

From fig(C) we get the relations:

$$R^2 = p^2 + x^2$$

$$r^2 = \frac{R^2}{4} + \rho^2 = \frac{p^2+x^2}{4} + \rho^2$$

Finally, the electronic energy loss for one collision at impact parameter p can be written:

$$T = \frac{m^2e^2}{4\pi^2\hbar^3}v\int_{-\infty}^{+\infty}[\int_0^{\infty}[\phi(\left(\frac{p^2+x^2}{4}+\rho^2\right)^{\frac{1}{2}}]^2\ 2\pi\rho d\rho dx \qquad \text{(II.55)}$$

The Firsov [Fir-1959] calculation of (II.55) by using the expression (II.54) for the potential ϕ gives

$$T = \frac{4.3\times10^{-8}(Z_1+Z_2)^{5/3}}{[1+3.1(Z_1+Z_2)^{\frac{1}{3}}10^7p]^5}v \qquad \text{(II.56)}$$

Where v is expressed in cm/sec and p in centimeters.

Thus, the Firsov's stopping power is obtained by the integral

$$S_e = \int d\sigma\, T(p) \qquad \text{(II.57)}$$

Where $d\sigma = 2\pi pdp$ represent the differential cross section, so by using (II.56) the equation (II.57) becomes

$$S_e = 2\pi\left(4.3\times10^{-8}(Z_1+Z_2)^{\frac{5}{3}}\right)\left(\int_0^{\infty}\frac{p}{\left[1+3.1(Z_1+Z_2)^{\frac{1}{3}}10^7p\right]^5}dp\right)\ v \qquad \text{(II.58)}$$

In order to resolve the above integral, we put

$$I_e = \int_0^{\infty}\frac{p}{[1+ap]^5}dp \qquad \text{(II.59)}$$

Where $a = 3.1(Z_1+Z_2)^{\frac{1}{3}}10^7$

Decomposing the integrant

$$\frac{p}{[1+ap]^5} = \frac{\alpha}{[1+ap]^4} + \frac{\beta}{[1+ap]^5}$$

We get by identification

$$\alpha = \frac{1}{a} \; and \; \beta = -\frac{1}{a}$$

So

$$\frac{p}{[1+ap]^5} = \frac{1}{a[1+ap]^4} - \frac{1}{a[1+ap]^5}$$

Thus

$$\int \frac{p}{[1+ap]^5}\, dx = \int \frac{1}{a[1+ap]^4}\, dx - \int \frac{1}{a[1+ap]^5}\, dx \qquad \text{(II.60)}$$

We put

$$I_1 = \int \frac{1}{a[1+ap]^4}\, dx \quad and \quad I_2 = \int \frac{1}{a[1+ap]^5}\, dx \qquad \text{(II.61)}$$

If we put $u = ax + 1$ so $dx = \frac{1}{a} du$ the tow integrals become

$$I_1 = \int \frac{1}{a^2 u^4}\, dx \quad and \quad I_2 = \int \frac{1}{a^2 u^5}\, dx \qquad \text{(II.62)}$$

Thus we get the solutions

$$I_1 = -\frac{1}{3a^2}\frac{1}{u^3} + C_1 \quad and \quad I_1 = -\frac{1}{4a^2}\frac{1}{u^4} + C_2 \qquad \text{(II.63)}$$

So

$$I_1 = -\frac{1}{3a^2}\frac{1}{[1+ap]^3} + C_1 \quad and \quad I_2 = -\frac{1}{4a^2}\frac{1}{[1+ap]^4} + C_2 \qquad \text{(II.64)}$$

Where C_1 and C_2 are constants.

Then we get

$$\int \frac{p}{[1+ap]^5}\, dx = I_1 - I_2 = -\frac{1}{3a^2}\frac{1}{[1+ap]^3} + \frac{1}{4a^2}\frac{1}{[1+ap]^4} + C \qquad \text{(II.65)}$$

Where C is a constant

The simplification of the above equation gives:

$$\int \frac{p}{[1+ap]^5}\, dx = -\frac{4ap+1}{12a^2[1+ap]^4} + C \qquad \text{(II.66)}$$

So,

$$I_e = \left[-\frac{4ap+1}{12a^2[1+ap]^4}\right]_0^{\infty} = \frac{1}{12a^2} \qquad \text{(II.67)}$$

$$I_e = \frac{1}{12\times(3.1(Z_1+Z_2)^{\frac{1}{3}}\times 10^7)^2} \qquad \text{(II.68)}$$

By inserting the solution obtained in equation (II.68) in (II.58) we get

$$S_e = \frac{2\pi\left(4.3\times10^{-8}(Z_1+Z_2)^{\frac{5}{3}}\right)}{12\times(3.1(Z_1+Z_2)^{\frac{1}{3}}\times10^7)^2}\ v \qquad \text{(II.69)}$$

The simplification of S_e gives:

$$S_e = 2.34\times10^{-23}(Z_1+Z_2)\ v \qquad \text{(II.70)}$$

If we introduce the Bohr velocity $v_0 = 2.2\ 10^8\ cm/s$ we get

$$S_e = 5.15\times10^{-15}(Z_1+Z_2)\ \frac{v}{v_0} \quad (\text{in } eV.cm^2/atom) \qquad \text{(II.71)}$$

6. Lindhard-Sharff-Schiott Stopping power model

Based on the statistical atomic model of Thomas and Fermi and other physical approaches, the LSS model is a theoretical rough description of ion implantation by Jens Lindhard, Morten Scharff and Hans E. Schiott [Lin-1963]. It offers analytical formula for the nuclear and the electronic stopping power of particles through matter in the low-velocity region $v \leq v_0 Z_1^{2/3}$ (LSS region), where v_0 represents the Bohr velocity and Z_1 the projectile atomic number. Recall that in this work, we are interested in the electronic stopping power. The LSS model supposes that quasi-elastic collisions occur between the ion and the target electrons as well as between the target atom and projectile electrons [Sig-2008]. The derivation of the LSS formula was never published, however some reasonable account are published later (for example Sugiyama who has shown that the LSS form for electronic stopping can be obtained following the procedure of Firsov (1981), and Tilinin in more recent papers (1995) [Nas-1996 & Sig-2008]).

According to [Lin-1963] the electronic stopping cross section per atom S_e is given by

$$S_e = -\frac{1}{N}\frac{dE}{dx} = \xi_e \cdot 8\pi e^2 a_0 \frac{Z_1 Z_2}{(Z_1^{\frac{2}{3}}+Z_2^{\frac{2}{3}})^{3/2}} \cdot \frac{v}{v_0}, v < v_1 = v_0 Z_1^{2/3} \qquad \text{(II.72)}$$

where N is the atomic density and the constant ξ_e was added as a fitting function to experimental data, it is of order of $Z_1^{1/6}$. Note that fluctuations around the constant ξ_e can occur, especially for $Z_1 \lesssim 10$ [Lin-1963].

In order to get the stopping power formula as $S(E) = \frac{1}{\rho}\frac{dE}{dx}$ where the unit of $S(E)$ is in $MeV \cdot cm^2 \cdot mg^{-1}$ and the kinetic energy of incident particle is in MeV per nucleon instead of its velocity v (v is proportional to the square root of the kinetic energy of the incident particle $\sqrt{E_k}$), we must carry out the development below:

since $N = \frac{N_A}{10^{-3}M_2}\rho$ so

$$S(E) = -\frac{1}{\rho}\frac{dE}{dx} = -\frac{N_A}{10^{-3}M_2}\frac{1}{N}\frac{dE}{dx} = \frac{N_A}{10^{-3}M_2}S_e$$

and since $E_k = \frac{1}{2}m_1 v^2$, where $m_1 = \frac{M_1}{N_A}$, we obtain

$$v = \sqrt{2\cdot10^3 N_A}\cdot\sqrt{E_k/M_1} = \sqrt{2\cdot10^3 N_A}\cdot\sqrt{E}$$

where $E = E_k/M_1$. After introducing the constant $\frac{1}{4\pi\varepsilon_0} = 9 \cdot 10^9 (SI)$ we get finally (in $MeV.cm^2/mg$):

$$S(E) = -\frac{1}{\rho}\frac{dE}{dx} = 73.226 \frac{{Z_1}^{1/6}}{M_2} \frac{Z_1 Z_2}{(Z_1^{\frac{2}{3}} + Z_2^{\frac{2}{3}})^{3/2}} \sqrt{E} \qquad \text{(II.73)}$$

The most important new feature of the LSS-theory was the clear recognition and identification of a wide range of particle energies where electronic and nuclear stopping were competing processes [Sig-1983].

7. Firsov verses LSS models

Both the Firsov and LSS formulas are proportional to the ion velocity i.e. the square root of the ion energy. The primary difference between the development of the Firsov and LSS models can be found in the choice of interatomic potential [Nas-1996].

The Firsov model assumes neutral collision partners and ignores ionization. Moreover, the electron current is assumed isotropic on the Firsov surface. This implies the stopping power reciprocity i.e. $S(Z_1\ in\ Z_2) = S(Z_2\ in\ Z_1)$ [Sig-2008]. On the other hand, it is clear that the empirical factor $\xi_e \sim Z_1^{1/6}$ appearing in the explicit LSS formula destroys the $Z_1 - Z_2$ symetry.

8. The software package SRIM (Stopping and Range of Ions in Matter)

Stopping and Range of Ions in Matter (SRIM) is a group of computer programs which calculate interaction of ions with matter [Zie-2013]. SRIM calculates the stopping and range of ions (10 eV - 10 GeV/amu) into matter using a full quantum mechanical treatment of ion-atom collisions. This calculation is made very efficient by the use of statistical algorithms which allow the ion to make jumps between calculated collisions and then averaging the collision results over the intervening gap. During the collisions, the ion and atom have a screened Coulomb collision, including exchange and correlation interactions between the overlapping electron shells. The ion has long range interactions creating electron excitations and plasmons within the target. These are described by including a description of the target's collective electronic structure and interatomic bond structure when the calculation is setup (tables of nominal values are supplied). The charge state of the ion within the target is described using the concept of effective charge, which includes a velocity dependent charge state and long range screening due to the collective electron sea of the target. A full description of the calculation is found in the tutorial book "***The Stopping and Range of Ions in Solids***" [Zie-2008].

SRIM will accept complex targets made of compound materials with up to eight layers, each of different materials. It will calculate all kinetic phenomena associated with the

ion's energy loss: target damage, sputtering, ionization, and phonon production. All target atom cascades in the target are followed in detail.

8.1. Stopping and Range Tables

The ion Stopping Tables gives values which are the same as those used in the Monte Carlo program TRIM. You may request stopping for any ion, with energies from 10 eV - 10 GeV, in both solid and gaseous targets made of complex materials. A variety of stopping units can be selected. The stopping powers were originally derived in 1984 using theoretical and experimental methods (see [Zie-2008]).

The ion Range Tables include both lists of the stopping powers, and also estimates of the ion range and its longitudinal and lateral straggle. These ranges are calculated using the program *PRAL*(*P*rojected *Ra*nge *Al*gorithm) by J. P. Biersack. This range calculation is remarkably accurate, and usually is within a few percent of the range values found using TRIM. The ranges calculated with TRIM should always be considered the benchmark, since the physical interaction between the ion and target atoms is considered in much more detail than in PRAL. If one wishes a table of ion ranges, one should consider obtaining a few ranges using Monte-Carlo TRIM and then interpolating using the tables of ranges produced by PRAL. The straggling values produced by PRAL are variable in accuracy, perhaps 20% for light ions, but up to 2 times for heavy ions.

8.2. Various versions of SRIM / TRIM

In this part we present different version of SRIM / TRIM with mention of changes in basic calculation without necessarily addressing the upgrade changes.

TRIM-85: Original release in 8/85.

TRIM-86: Major change made in definition of cascade displacements and vacancies to make it agree closely with the assumptions of Kinchin and Pease.

TRIM-87: Added transverse straggling of the ions, and ion sputtering of the surface. Corrected many small bugs in various plots. Changed ion stopping in silicon for Z1<19 because of much new data.

TRIM-88: TRIM has been converted to Turbo-BASIC from the original FORTRAN. This will allow the use of Enhanced Graphics for future versions. A table of common compounds has been added for convenience. Ion energies up to 2 GeV/amu now available.

TRIM-89: A large dictionary of COMPOUNDS has been integrated into the programs. The stopping of ions in compounds is executed using the formalism described in "The Stopping of

Ions in Compounds".

TRIM-90: EGA three-dimensional TRIM- First general release, Feb.,1990.

SRIM-91: Corrected bug in COLLISON.TXT which listed wrong primary collison atom.

Added lateral distribution to file COLLISON.TXT.

Corrected statistical range distribution moments (H. Glawishnig, Siemens).

Revised Skewness and Kurtosis to fit VLSI modelling conventions.

Remark:

"TRIM-xx" renamed **"SRIM-xx"** in 1991 to end confusion between the Monte Carlo program TRIM and package of programs titled TRIM-xx.

SRIM-95: Comprehensive change in all Ion Stopping Powers. New theory for heavy ions. Reluctantly, stopping in gases is also included, although not too accurate.

SRIM-2000: Incorporated new high energy stopping power theory (E>1 MeV/u) in SR. Corrected bug in SR calculation of He, Li stopping in heavy gases.

SRIM-2003: Totally new stopping powers, with significant improvement for Heavy Ions. Introduction of Nuclear Stopping using specific atom/atom calculations. Extended Max Energy to 10 GeV/u, plus fixed a few small bugs.

SRIM-2006: Upgrade but no changes to basic calculation of SRIM-2003

SRIM-2008: Made changes to sputtering of targets Z=13 to21 to omit discontinuity in treatment.

SRIM-2013: Several bugs corrected, including bugs in Compound Dictionary.

It is clear that SRIM is in a remarkable changes and developments according to the availability and development of theoretical and empirical data, which in turn still know a great shortage and discrepancies.

9. Conclusion

In this chapter, we have presented the cross section concept and a general expression of the stopping power, then the two models of Firsov and Lindhard-Sharff-Schiott (LSS) of stopping power at low ion velocities that represent the subject of this work, and a comparison between them. Finally, we give a presentation of the software package SRIM (Stopping and Range of Ions in Matter) which is based on theoretical treatment of ion-atom collisions and available data.

Chapter III

Results and Discussion

1. Introduction

In this chapter, we calculate the stopping power values generated by the Firsov and LSS model and compare them to those published by H. Paul data base as well as to those predicted with SRIM programm for ions-targets couples ^{12}Mg in ^{6}C, ^{12}Mg in ^{22}Ti, ^{12}Mg in ^{47}Ag, ^{17}Cl in ^{6}C, ^{17}Cl in ^{13}Al, ^{17}Cl in ^{28}Ni, ^{17}Cl in ^{79}Au, ^{22}Ti in ^{6}C, ^{22}Ti in ^{13}Al, ^{22}Ti in ^{29}Cu, ^{22}Ti in ^{79}Au, ^{29}Cu in ^{6}C, ^{29}Cu in ^{13}Al, ^{29}Cu in ^{29}Cu, ^{23}Cu in ^{79}Au, ^{36}Kr in ^{6}C, ^{36}Kr in ^{28}Ni, ^{36}Kr in ^{79}Au, ^{47}Ag in^{13}Al, ^{47}Ag in ^{30}Zn, and ^{47}Ag in ^{46}Pd. We discuss also the Z oscillations which are due to the shell structure of the atoms.

2. Stopping powers of the projectile ^{12}Mg

In figure III.1 we plot the stopping power of ^{12}Mg in ^{6}C, ^{12}Mg in ^{22}Ti and ^{12}Mg in ^{47}Ag deduced from LSS and Firsov calculation. To compare the calculate values of stopping power we introduce in Fig. III.1 some available data of stopping power. The experimental data of stopping power are taken from ref. [Fas-1966] for ^{12}Mg in ^{6}C and from ref. [Ars-1990] for ^{12}Mg in ^{22}Ti and ^{12}Mg in ^{47}Ag.

From Fig. III.1, we can conclude that:

- In general, no discrepancies between SRIM simulation and available data,
- At low velocity region a good correlation between the Firsov's models and available dada as well as with SRIM simulation for ^{12}Mg in ^{6}C and ^{12}Mg in ^{47}Ag.
- For ^{12}Mg in ^{22}Ti a deviation up to 20% between Firsov model and available data.
- An appreciable deviation between LSS and available data for ^{12}Mg in ^{6}C and ^{12}Mg in ^{47}Ag as well as ^{12}Mg in ^{22}Ti.

Can we conclude, for a projectile like magnesium (from point of view atomic number Z_1), that the two models are more compatible with the relatively lighter atoms (Z_2

relatively close to carbon) and relatively heavier atoms (Z_2 relatively close to ^{47}Ag) contrary to the intermediate atoms between them (e.g. ^{22}Ti)?

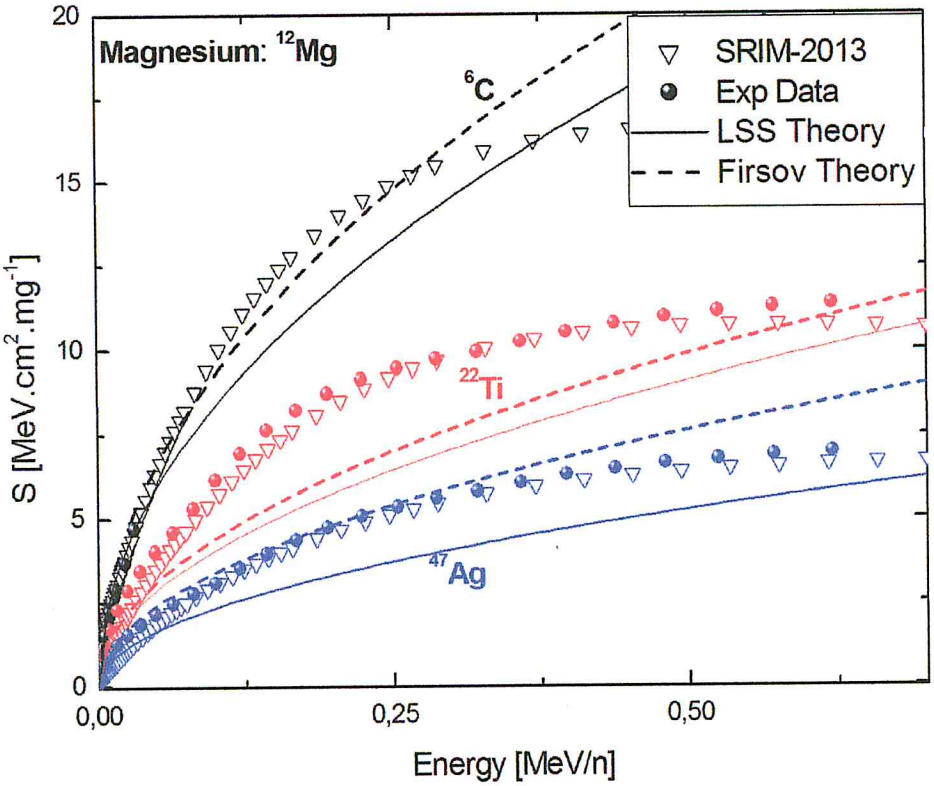

Fig. III.1 : Comparison of stopping power data [Paul-2013] (circle) for ^{12}Mg in ^{6}C, ^{12}Mg in ^{22}Ti, and ^{12}Mg in ^{47}Ag with Firsov theory (dashed lines), LSS formula (solid lines) and the well knows SRIM code [Zei-2013].

3. Stopping powers of the projectile ^{17}Cl

In figure III.2 we plot the stopping power of ^{17}Cl in ^{6}C, ^{17}Cl in ^{13}Al, ^{17}Cl in ^{28}Ni and ^{17}Cl in ^{79}Au deduced from LSS and Firsov calculation. For comparison of the calculate values of stopping power we include in Fig. III.2 some available experimental data from different references data. The experimental of stopping power data of ^{17}Cl in ^{6}C are obtained by direct transmission method using carbon foils of about 20 $\mu g.cm^{-2}$ of thicknesses [Fas-1966] and [Boo-1965]. The stopping power data of ^{17}Cl in ^{13}Al, ^{17}Cl in ^{28}Ni and ^{17}Cl in ^{79}Au are obtained by direct transmission using uniform foils with 2% thickness uncertainty and with calibration uncertainties 3% [Boo-1965].

From Fig. III.2, in the same manner as Fig. III.1, we can conclude that:

- In general, no discrepancies between SRIM simulation and available data.
- At low velocity region a good correlation between the Firsov's models and available dada as well as with SRIM simulation for ^{17}Cl in ^{6}C and ^{17}Cl in ^{79}Au with a slight deviation for ^{79}Au.
- Both models are identical for ^{17}Cl in ^{13}Al and ^{17}Cl in ^{28}Ni, but the compatibility with experimental dada as well as with SRIM simulation is higher for ^{17}Cl in ^{28}Ni than ^{17}Cl in ^{13}Al.

Since the two models are based on the statistical Thomas-Fermi atomic model, is this behavior due to the difference between the two atoms in the shell structure?

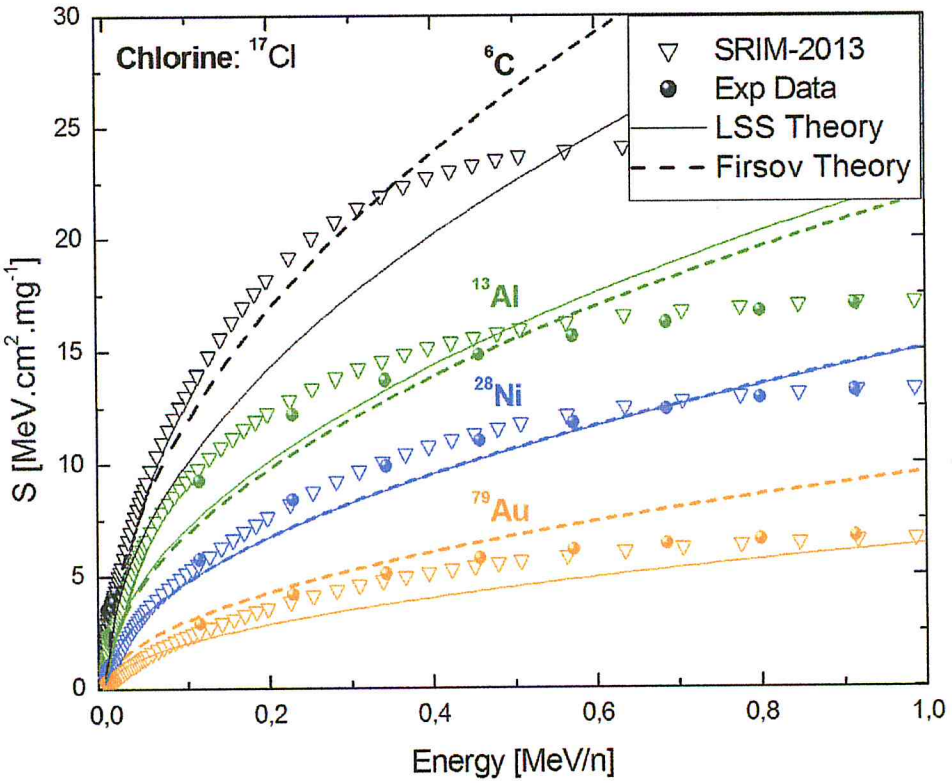

Fig. III.2: Same as in Fig. III.1, but for ^{17}Cl in ^{6}C, ^{17}Cl in ^{13}Al, ^{17}Cl in ^{28}Ni and ^{17}Cl in ^{79}Au.

4. Stopping powers of the projectile ^{22}Ti

In figure III.3 we plot the stopping power of ^{22}Ti in ^{6}C, ^{22}Ti in ^{13}Al, ^{22}Ti in ^{29}Cu and ^{22}Ti in ^{79}Au deduced from LSS and Firsov calculation as well as available data in parallel with SRIM computation.

The stopping power of ^{22}Ti in ^{6}C was deduced from the measurement of the ranges of Ti/C for 26 different implantation energies [Sch-1991].

The stopping power data of ^{22}Ti in ^{13}Al, ^{22}Ti in ^{29}Cu and ^{22}Ti in ^{79}Au are measured by direct transmission [Gei-1983]. The stopping power at an energy E is obtained by dividing the energy loss ΔE in the target by the target thickness ΔE. The energy E is obtained from the incident energy E_0 by: $E=E_0-\Delta E/2$. Some of stopping power data of ^{22}Ti in ^{13}Al are obtained by using a time of flight spectrometer [Gei-1982]. The overall uncertainty of the measured stopping powers (S) in solids was obtained from the variance of S for different targets of the same element and found to be smaller than 5%.

From Fig. III.3, we can conclude that:

- In general, the LSS and Firsov's models give identical results except for Ti in C, where the Firsov's model is in good agreement with available dada as well as with SRIM predictions and the LSS model goes farther away.
- At low velocity region there is good correlation between the two models and available dada as well as with SRIM predictions for ^{22}Ti in ^{29}Cu and ^{22}Ti in ^{79}Au.
- For ^{22}Ti in ^{13}Al there is relatively large deviation from experimental dada as well as with SRIM predictions.

Can we conclude that this deviation is due to the shells effect of Al?

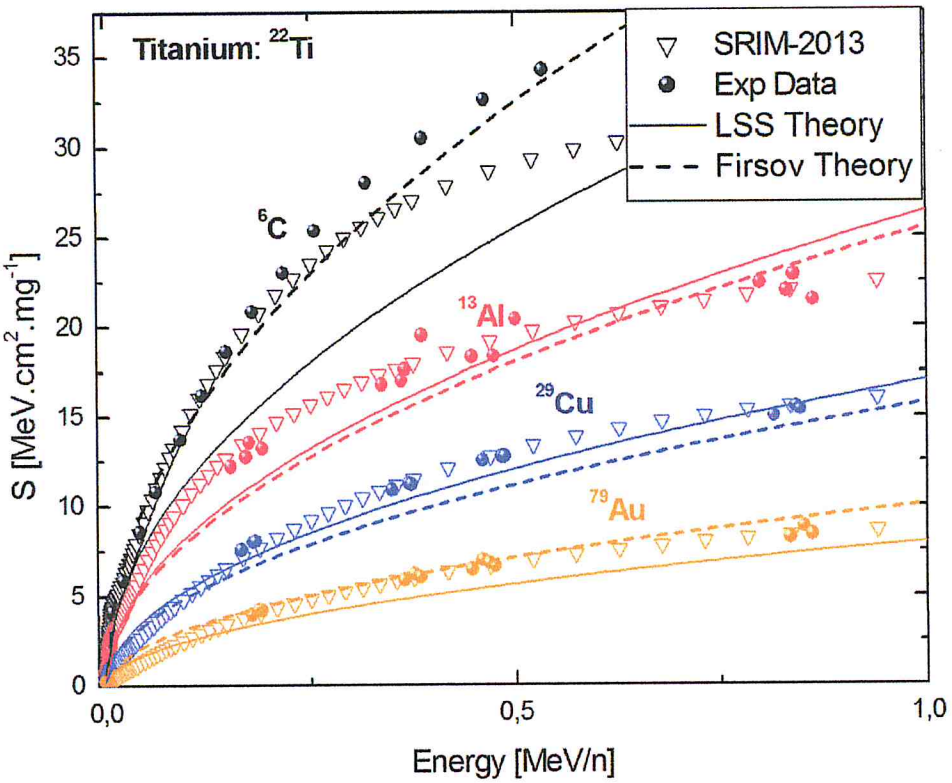

Fig.III.3: Same as in Fig. III.1, but for ^{22}Ti in ^{6}C, ^{22}Ti in ^{13}Al, ^{22}Ti in ^{29}Cu and ^{22}Ti in ^{79}Au.

5. Stopping powers of the projectile ^{29}Cu

In figure III.4 we plot the stopping power of for ^{63}Cu in ^{12}C, ^{63}Cu in ^{27}Al, ^{63}Cu in ^{63}Cu and ^{63}Cu in ^{197}Au deduced from LSS and Firsov calculation as well as available data in parallel with SRIM computation.

The experimental data of stopping power for ^{63}Cu in ^{12}C are obtained by using modified time-of-flight-energy elastic recoil detection analysis (ToF-E ERDA) set-up [Zha-2002]. For ^{63}Cu in ^{63}Cu, the experimental procedure consist of using non-conventional ERDA methods, and spectrometers to separate signals of different elements and isotopes from each other [Jok-1997]. The experimental data of ^{63}Cu in ^{197}Au are obtained by interposing thin self-supporting foils of known areal density in the trajectory of the secondary beam. The stopping data are assigned an uncertainty of 5 % [Abd-1992-c].

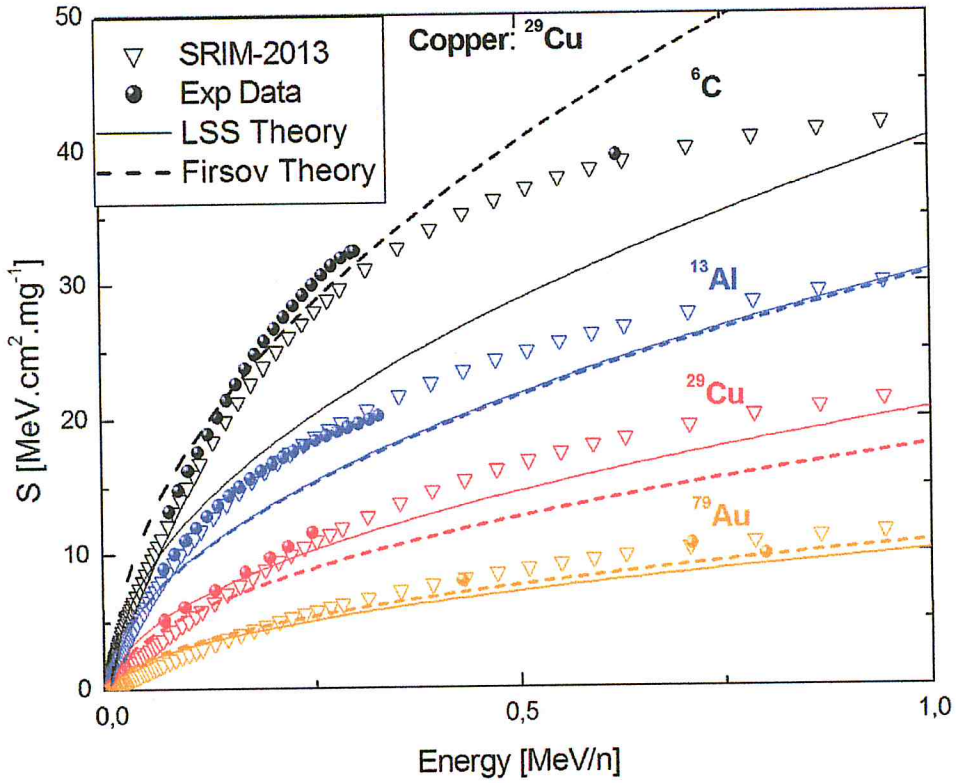

Fig. III.4: Same as in Fig. III.1, but for ^{63}Cu in ^{12}C, ^{63}Cu in ^{27}Al, ^{63}Cu in ^{63}Cu and ^{63}Cu in ^{197}Au.

From Fig. III.4, we can conclude that:

- For ^{29}Cu in ^{6}C the Firsov's model always in agreement with experimental data as well as SRIM predictions while the LSS model deviates considerably.
- For ^{23}Cu in ^{79}Au, the two models are approaching the experimental data as well as the SRIM predictions.
- For ^{29}Cu in ^{29}Cu the LSS model only approaches, while for ^{29}Cu in ^{13}Al the two models are identical but not in agreement with available data as well as SRIM predictions.

6. Stopping powers of the projectile ^{36}Kr

In figure III.5 we plot the stopping power of in ^{36}Kr in ^{6}C, ^{36}Kr in ^{28}Ni, and ^{36}Kr in ^{79}Au deduced from LSS and Firsov calculation as well as available data in parallel with SRIM computation. The experimental data of stopping power are taken from ref. [Pap-1978] for ^{36}Kr in ^{6}C and from ref. [Gei-1982 & Gei-1983] for ^{36}Kr in ^{28}Ni and ^{36}Kr in ^{79}Au. The

experimental protocol followed by [Gei-1982] and [Gei-1983] is well discussed above in section 4.

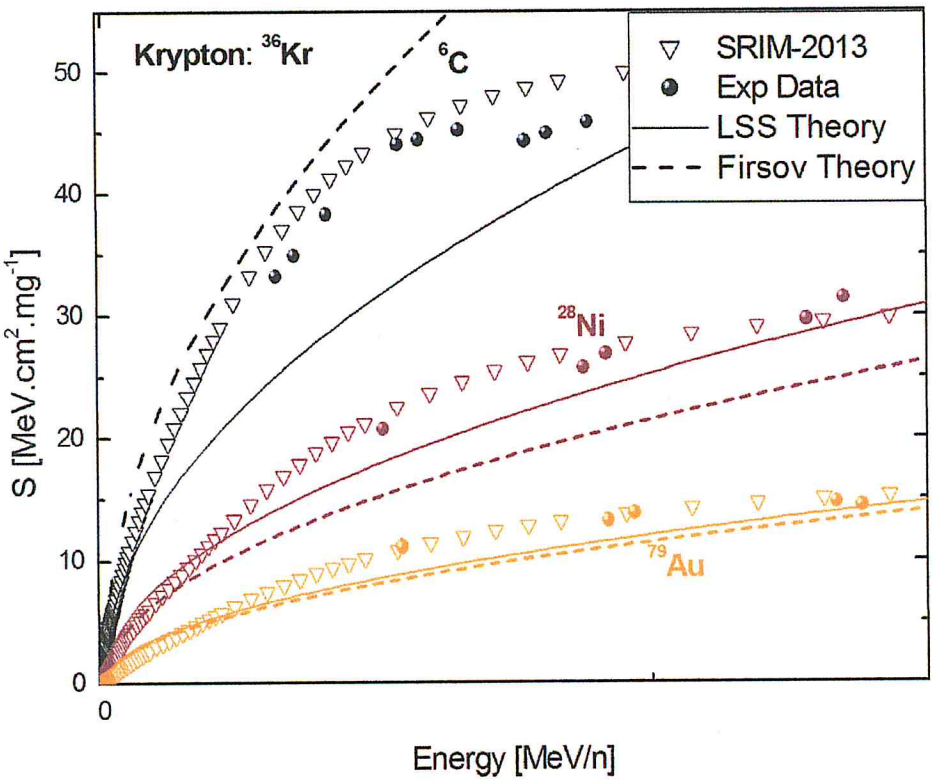

Fig. III.5: Same as in Fig. III.1 but for ^{36}Kr in ^{12}C, ^{36}Kr in ^{28}Ni, and ^{36}Kr in ^{79}Au .

From Fig. III.5, we can conclude that:

- For the stopping power of ^{36}Kr in ^{6}C, the Firsov's model is nearly in agreement with the SRIM predictions but not with experimental data which show some discrepancies, while the LSS model shows significant deviation from the SRIM predictions.
- For ^{36}Kr in ^{79}Au, the two models are identical and almost in agreement with available data as well as SRIM predictions.
- For ^{36}Kr in ^{28}Ni the LSS model does not go too far the experimental and the SRIM predictions while the Firsov's model goes farther away.

7. Stopping powers of the projectile ^{47}Ag

In figure III.6 we plot the stopping power of ^{47}Ag in ^{13}Al, ^{47}Ag in ^{30}Zn, and ^{47}Ag in ^{46}Pd deduced from LSS and Firsov calculation calculation as well as available data in parallel

with SRIM computation. The experimental data of ^{47}Ag in ^{13}Al were measured in the transmission mode by interposing thin foils of known thickness into the trajectory of a secondary beam [Abd-1992-a] The experimental data of stopping power are taken from ref. [Rib-1983] for ^{47}Ag in ^{30}Zn, and ^{47}Ag in ^{46}Pd.

From Fig. III.6, we can conclude that:

- For the stopping powers of ^{47}Ag projectile, we observe a greater divergence between the two models and experimental data as well as SRIM predictions compared to the previous projectiles.
- For ^{47}Ag in^{13}Al, there are discrepancies between SRIM predictions and experimental data.
- For ^{47}Ag in ^{30}Zn, and ^{47}Ag in ^{46}Pd, the Firsov's model goes farther from the available data as well SRIM predictions than the LSS model.
- For ^{47}Ag in^{13}Al, the LSS model go farther from the available data as well SRIM predictions than the Firsov's model.

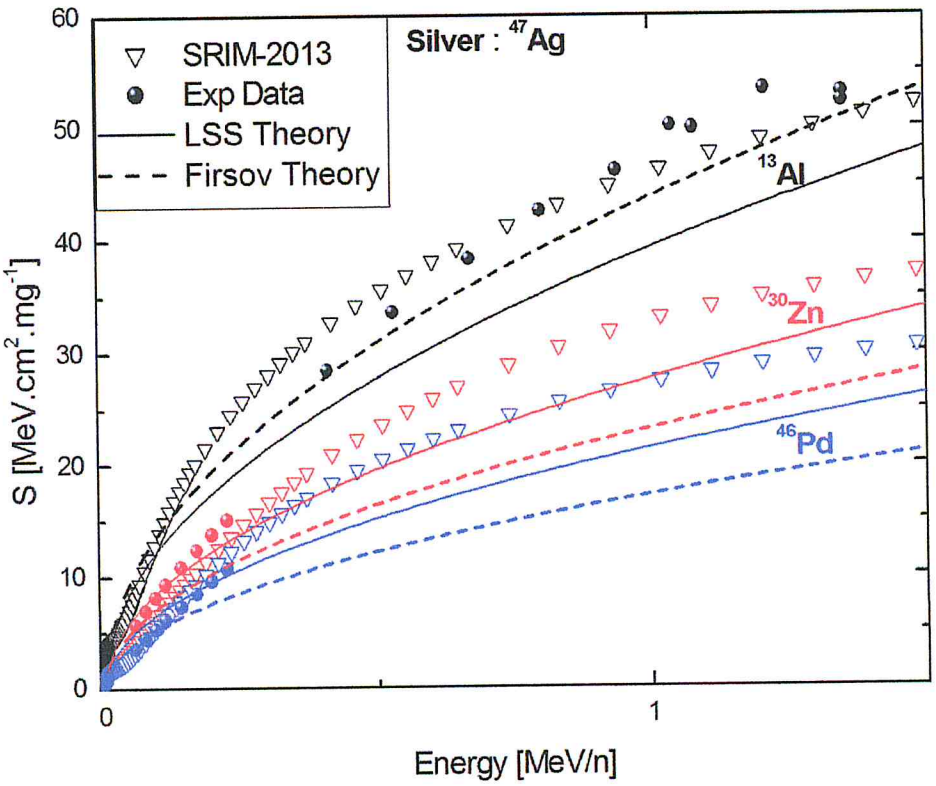

Fig. III.6: Same as in Fig. III.1 but for for ^{47}Ag in ^{13}Al, ^{47}Ag in ^{30}Zn, and ^{47}Ag in ^{46}Pd.

8. Numerical tables of the previous data

These tables present the numerical values of the experimental data schematized in the previous graphs and the deviation percentages of the two models in relation to the available data.

Energy MeV/n	S SRIM	S Exp	S LSS	S Fir	Dev/LSS %	Dev/Fir %
Data [Fas-1966] Mg on C (all S units are in MeV.cm^2.mg^{-1})						
0,0054	1,69	1,50	1,95	2,17	-30	-44
0,0074	1,96	1,82	2,28	2,54	-25	-39
0,0094	2,23	2,21	2,57	2,87	-16	-30
0,0114	2,48	2,49	2,83	3,15	-14	-27
0,0150	2,89	2,89	3,25	3,61	-12	-25
0,0229	3,75	3,67	4,01	4,46	-09	-22
0,0306	4,55	4,68	4,64	5,16	01	-10

Table III.1.a: Numerical comparison of stopping power data [Paul-2013] for ^{12}Mg in ^{6}C with Firsov theory and LSS formula

Energy MeV/n	S SRIM	S Exp	S LSS	S Fir	Dev/LSS %	Dev/Fir %
Data [Ars-1990]Mg on Ti (all S units are in MeV.cm^2.mg^{-1})						
0,0010	0,25	0,57	0,40	0,44	29	23
0,0040	0,61	1,15	0,81	0,88	30	23
0,0089	0,94	1,72	1,21	1,32	29	23
0,0159	1,47	2,29	1,62	1,76	29	23
0,0248	2,09	2,87	2,02	2,20	29	23
0,0357	2,75	3,44	2,43	2,64	29	23
0,0486	3,44	4,01	2,83	3,08	29	23
0,0635	4,15	4,59	3,24	3,52	29	23
0,0804	4,88	5,30	3,64	3,96	31	25
0,0992	5,61	6,15	4,05	4,40	34	28
0,1200	6,33	6,93	4,45	4,84	36	30
0,1429	7,03	7,63	4,86	5,28	36	31
0,1677	7,68	8,22	5,26	5,72	36	30
0,1944	8,28	8,72	5,67	6,16	35	29
0,2232	8,81	9,13	6,07	6,60	34	28
0,2540	9,27	9,46	6,48	7,04	32	26
0,2867	9,67	9,73	6,88	7,48	29	23
0,3214	9,98	9,94	7,28	7,92	27	20
0,3581	10,24	10,24	7,69	8,36	25	18
0,3968	10,44	10,53	8,09	8,80	23	16
0,4375	10,59	10,78	8,50	9,25	21	14
0,4801	10,69	10,98	8,90	9,69	19	12
0,5248	10,75	11,15	9,31	10,13	17	09
0,5714	10,77	11,28	9,71	10,57	14	06
0,6200	10,76	11,38	10,12	11,01	11	03

Table III.1.b: Numerical comparison of stopping power data [Paul-2013] for ^{12}Mg in ^{22}Ti with Firsov theory and LSS formula

From table III.1.a we can see that the deviation percentages are up to 30 % for the LSS model and up to 44 % for the Firsov's model. At very low velocities, where the nuclear stopping power is not negligible, the deviations of the two models from available data are much higher; this is probably due to fact that in the Firsov's and LSS's models the nuclear stopping power is not taken into account.

From table III.1.b we can see that the deviation percentages are up to 36 % for the LSS model and up to 31 % for the Firsov's model. Also we remark considerable deviations for very low velocities.

Energy MeV/n	S SRIM	S Exp	S LSS	S Fir	Dev/LSS %	Dev/Fir %
Data [Ars-1990]Mg on Ag (all S units are in MeV.cm^2.mg^{-1})						
0,0010	0,13	0,31	0,23	0,34	25	-09
0,0040	0,31	0,61	0,47	0,68	24	-11
0,0089	0,47	0,92	0,70	1,02	24	-11
0,0159	0,74	1,23	0,93	1,36	24	-10
0,0248	1,08	1,53	1,16	1,70	24	-11
0,0357	1,44	1,84	1,40	2,03	24	-11
0,0486	1,83	2,15	1,63	2,37	24	-10
0,0635	2,22	2,45	1,86	2,71	24	-11
0,0804	2,62	2,76	2,10	3,05	24	-11
0,0992	3,02	3,08	2,33	3,39	24	-10
0,1200	3,41	3,52	2,56	3,73	27	-06
0,1429	3,80	3,95	2,79	4,07	29	-03
0,1677	4,17	4,35	3,03	4,41	30	-01
0,1945	4,51	4,72	3,26	4,75	31	-01
0,2232	4,84	5,05	3,49	5,09	31	-01
0,2540	5,14	5,33	3,73	5,42	30	-02
0,2867	5,41	5,58	3,96	5,76	29	-03
0,3214	5,65	5,78	4,19	6,10	27	-06
0,3581	5,86	6,04	4,42	6,44	27	-07
0,3968	6,05	6,27	4,66	6,78	26	-08
0,4375	6,21	6,46	4,89	7,12	24	-10
0,4802	6,34	6,62	5,12	7,46	23	-13
0,5248	6,45	6,75	5,36	7,80	21	-16
0,5714	6,54	6,86	5,59	8,14	19	-19
0,6201	6,61	6,95	5,82	8,48	16	-22

Table III.1.c: Numerical comparison of stopping power data [Paul-2013] for ^{12}Mg in ^{47}Ag with Firsov theory and LSS formula.

From table III.1.c we can see that the deviation percentages are up to 31 % for the LSS model and up to 22 % for the Firsov's model. We see that in many cases the Firsov's deviations are smaller than the LSS deviations.

Energy MeV/n	S SRIM	S Exp	S LSS	S Fir	Dev/LSS %	Dev/Fir %
Data [Fas-1966] Cl on C (all S units are in MeV.cm^2.mg^{-1})						
0,004	3,44	2,34	1,97	2,33	16	00
0,005	3,54	2,82	2,31	2,73	18	03
0,007	3,66	3,21	2,61	3,09	19	04
0,008	3,79	3,53	2,86	3,39	19	04
0,010	4,08	3,87	3,24	3,83	16	01
0,013	4,46	4,34	3,64	4,31	16	01

Table III.2.a: Numerical comparison of stopping power data [Paul-2013] for ^{17}Cl in ^{6}C with Firsov theory and LSS formula.

From table III.2.a we can see that the deviation percentages are up to 19 % for the LSS model and up to 04 % for the Firsov's model. It seems that the Firsov's deviations are smaller than the LSS deviations and that the Firsov's model is in good agreement with available data, but it should not be forgotten that these are the ranges of low energies, where the nuclear stopping powers take non-negligible values compared to the electronic stopping powers.

Energy MeV/n	S SRIM	S Exp	S LSS	S Fir	Dev/LSS %	Dev/Fir %
Data [Boo-1965] Cl on Al (all S units are in MeV.cm².mg^{-1})						
0,114	9,85	9,26	7,66	7,40	17	20
0,229	12,90	12,20	10,83	10,46	11	14
0,343	14,59	13,70	13,26	12,81	03	06
0,457	15,60	14,80	15,31	14,79	-03	00
0,571	16,24	15,60	17,12	16,54	-10	-06

Table III. 2.b: Numerical comparison of stopping power data [Paul-2013] for ^{17}Cl in ^{13}Al with Firsov theory and LSS formula.

From table III.2.b we can see that the deviation percentages are up to 17 % for the LSS model and up to 20 % for the Firsov's model.

Energy MeV/n	S SRIM	S Exp	S LSS	S Fir	Dev/LSS %	Dev/Fir %
Data [Boo-1965] Cl on Ni (all S units are in MeV.cm².mg^{-1})						
0,114	5,57	5,76	5,09	5,10	12	11
0,229	8,27	8,40	7,20	7,21	14	14
0,343	10,12	9,90	8,82	8,83	11	11
0,457	11,36	11,00	10,18	10,20	07	07
0,571	12,17	11,80	11,38	11,41	04	03
0,686	12,70	12,40	12,47	12,49	-01	-01
0,800	13,03	12,90	13,47	13,49	-04	-05

Table III.2.c: Numerical comparison of stopping power data [Paul-2013] for ^{17}Cl in ^{28}Ni with Firsov theory and LSS formula.

From table III.2.c we can see that the deviation percentages are up to 14 % for the LSS model and up to 20 % for the Firsov's model.

Energy MeV/n	S SRIM	S Exp	S LSS	S Fir	Dev/LSS %	Dev/Fir
Data [Boo-1965] Cl on Au						
0,114	2,55	2,89	2,15	3,24	25	-12
0,229	3,90	4,20	3,05	4,59	27	-09
0,343	4,81	5,10	3,73	5,62	27	-10
0,457	5,44	5,75	4,31	6,48	25	-13
0,571	5,87	6,13	4,82	7,25	21	-18
0,686	6,18	6,40	5,28	7,94	18	-24
0,800	6,39	6,58	5,70	8,58	13	-30
0,914	6,55	6,72	6,09	9,17	09	-36

Table III.2.d: Numerical comparison of stopping power data [Paul-2013] for ^{17}Cl in ^{79}Au with Firsov theory and LSS formula.

From table III.2.d we can see that the deviation percentages are up to 27 % for the LSS model and up to 36 % for the Firsov's model. We remark that in contrary to the results of the LSS model, the deviations of the results of the Firsov's model in relation to the available data increase as a function of the energy of the incident particle (Cl).

Energy MeV/n	S SRIM	S Exp	S LSS	S Fir	Dev/LSS %	Dev/Fir %
Data [Sch-1991] Ti on C (all S units are in MeV.cm^2.mg^{-1})						
0,01	4,39	4,15	3,21	4,09	23	01
0,02	5,93	5,88	5,31	6,77	10	-15
0,04	8,52	8,57	7,40	9,42	14	-10
0,06	10,86	10,79	8,92	11,36	17	-05
0,09	1,40	13,69	10,88	13,86	21	-01
0,12	16,28	16,20	12,36	15,74	24	03
0,15	18,42	18,64	13,83	17,62	26	05
0,18	20,33	20,85	15,27	19,45	27	07
0,22	22,17	22,99	16,80	21,39	27	07
0,26	23,72	25,35	18,23	23,22	28	08
0,32	25,70	28,04	20,36	25,93	27	08
0,39	27,28	30,51	22,45	28,59	26	06
0,46	28,56	32,61	24,55	31,26	25	04
0,54	29,45	34,26	26,37	33,57	23	02

Table III.3.a: Numerical comparison of stopping power data [Paul-2013] for ^{22}Ti in ^{6}C with Firsov theory and LSS formula.

From table III.3.a we can see that the deviation percentages are up to 28 % for the LSS model and up to 15 % for the Firsov's model.

Energy MeV/n	S SRIM	S Exp	S LSS	S Fir	Dev/LSS %	Dev/Fir %
Data [Gei-1982 & Gei-1983] Ti on Al (all S units are in MeV.cm^2.mg^{-1})						
0,15	12,88	12,22	10,32	9,97	16	18
0,17	13,55	12,74	10,94	10,56	14	17
0,18	13,67	13,56	11,06	10,68	18	21
0,19	14,18	13,22	11,56	11,16	13	16
0,34	17,35	16,81	15,36	14,82	09	12
0,36	17,74	17,02	15,91	15,35	07	10
0,37	17,80	17,62	15,99	15,43	09	12
0,39	18,10	19,52	16,44	15,87	16	19
0,45	18,89	18,32	17,69	17,07	03	07
0,47	19,21	18,33	18,21	17,58	01	04
0,50	19,49	20,39	18,71	18,06	08	11
0,80	21,83	22,41	23,63	22,81	-05	-02
0,83	22,01	21,97	24,11	23,27	-10	-06

Table III.3.b: Numerical comparison of stopping power data [Paul-2013] for ^{22}Ti in ^{13}Al with Firsov theory and LSS formula.

From table III.3.b we can see that the deviation percentages are up to 18 % for the LSS model and up to 21 % for the Firsov's model.

Energy MeV/n	S SRIM	S Exp	S LSS	S Fir	Dev/LSS %	Dev/Fir %
Data [Gei-1982 & Gei-1983] Ti on Cu (all S units are in MeV.cm^2.mg^{-1})						
0,17	7,10	7,60	6,93	6,42	09	16
0,18	7,50	8,00	7,23	6,70	10	16
0,18	7,56	8,05	7,28	6,75	10	16
0,35	11,05	10,90	10,08	9,33	08	14
0,37	11,37	11,26	10,37	9,60	08	15
0,37	11,42	11,19	10,41	9,65	07	14
0,46	12,61	12,52	11,57	10,71	08	14
0,48	12,89	12,74	11,86	10,98	07	14
0,49	12,93	12,74	11,90	11,02	07	13
0,82	15,51	15,02	15,40	14,26	-03	05
0,84	15,64	15,55	15,64	14,49	-01	07
0,85	15,66	15,38	15,69	14,53	-02	06

Table III.3.c: Numerical comparison of stopping power data [Paul-2013] for ^{22}Ti in ^{29}Cu with Firsov theory and LSS formula.

From table III.3.c we can see that the deviation percentages are up to 10 % for the LSS model and up to 16 % for the Firsov's model.

The same conclusion as before we can see from the following table III.3.d that the deviation percentages are up to 22 % for the LSS model and up to 11 % for the Firsov's model.

Energy MeV/n	S SRIM	S Exp	S LSS	S Fir	Dev/LSS %	Dev/Fir %
Data [Gei-1982 & Gei-1983] Ti on Au (all S units are in MeV.cm².mg^{-1})						
0,1774	3,905	3,98	3,37	4,25	15	-07
0,1862	4,029	4,23	3,45	4,35	18	-03
0,1912	4,097	4,21	3,50	4,41	17	-05
0,3646	5,916	5,9	4,83	6,09	18	-03
0,3768	6,017	6,22	4,91	6,19	21	00
0,3842	6,037	6,05	4,96	6,25	18	-03
0,4474	6,535	6,48	5,35	6,75	17	-04
0,4602	6,624	7	5,43	6,85	22	02
0,4684	6,68	6,81	5,48	6,91	20	-01
0,4756	6,726	6,67	5,52	6,96	17	-04
0,8344	8,353	8,25	7,31	9,22	11	-12
0,8506	8,398	8,84	7,38	9,31	16	-05
0,8608	8,426	8,4	7,43	9,36	12	-11

Table III.3.d: Numerical comparison of stopping power data [Paul-2013] for ^{22}Ti in ^{79}Au with Firsov theory and LSS formula.

Energy MeV/n	S SRIM	S Exp	S LSS	S Fir	Dev/LSS %	Dev/Fir %
Data [Zha-2002] Cu on C (all S units are in MeV.cm².mg^{-1})						
0,07	12,37	13,22	10,96	15,43	17	-17
0,08	13,81	14,79	11,82	16,64	20	-13
0,10	15,19	16,24	12,62	17,77	22	-09
0,11	16,50	17,61	13,37	18,83	24	-07
0,12	17,73	18,93	14,09	19,83	26	-05
0,13	18,92	20,21	14,76	20,79	27	-03
0,14	20,05	21,44	15,41	21,70	28	-01
0,16	21,11	22,62	16,04	22,58	29	00
0,17	22,12	23,74	16,64	23,42	30	01
0,18	23,08	24,79	17,21	24,23	31	02
0,19	23,99	25,78	17,77	25,02	31	03
0,20	24,84	26,71	18,32	25,79	31	03
0,21	25,65	27,58	18,84	26,53	32	04
0,23	26,42	28,41	19,36	27,25	32	04
0,24	27,16	29,21	19,85	27,95	32	04
0,25	27,85	29,98	20,34	28,64	32	04
0,26	28,50	30,71	20,82	29,31	32	05
0,27	29,13	31,39	21,28	29,96	32	05
0,28	29,73	31,97	21,74	30,60	32	04
0,30	30,27	32,37	22,18	31,23	31	04
0,30	30,49	32,45	22,36	31,48	31	03
0,62	38,98	39,53	32,12	45,22	19	-14

Table III.4.a: Numerical comparison of stopping power data [Paul-2013] for ^{63}Cu in ^{12}C with Firsov theory and LSS formula.

Also from the table III.4.a, the deviation percentages are up to 32 % for the LSS model and up to 17 % for the Firsov's model.

Energy MeV/n	S SRIM	S Exp	S LSS	S Fir	Dev/LSS %	Dev/Fir %
Data [Zha-2002] Cu on Al (all S units are in MeV.cm^2.mg^{-1})						
0,07	8,25	8,95	7,88	7,82	12	13
0,08	9,39	10,03	8,64	8,58	14	14
0,09	10,45	11,04	9,35	9,28	15	16
0,11	11,42	11,98	10,00	9,93	17	17
0,12	12,32	12,85	10,61	10,54	17	18
0,13	13,16	13,64	11,19	11,11	18	18
0,14	13,94	14,36	11,74	11,66	18	19
0,16	14,67	15,02	12,27	12,18	18	19
0,17	15,34	15,62	12,78	12,68	18	19
0,18	15,98	16,18	13,26	13,17	18	19
0,20	16,57	16,70	13,73	13,63	18	18
0,21	17,14	17,19	14,18	14,08	17	18
0,22	17,67	17,64	14,62	14,52	17	18
0,24	18,17	18,05	15,05	14,94	17	17
0,25	18,65	18,43	15,46	15,35	16	17
0,26	19,10	18,77	15,86	15,75	15	16
0,28	19,53	19,09	16,26	16,14	15	15
0,29	19,94	19,37	16,64	16,52	14	15
0,30	20,33	19,65	17,02	16,90	13	14
0,32	20,72	19,95	17,39	17,26	13	13
0,33	21,00	20,22	17,67	17,55	13	13

Table III.4.b: Numerical comparison of stopping power data [Paul-2013] for ^{63}Cu in ^{27}Al with Firsov theory and LSS formula.

The table III.4.b indicates that the deviation percentages are up to 18 % for the LSS model and up to 19 % for the Firsov's model.

Energy MeV/n	S SRIM	S Exp	S LSS	S Fir	Dev/LSS %	Dev/Fir %
Data [Jok-1997] Cu on Cu (all S units are in MeV.cm^2.mg^{-1})						
0,07	3,75	5,11	5,26	4,58	-03	10
0,09	4,92	6,07	6,21	5,41	-02	11
0,13	6,49	7,34	7,35	6,40	00	13
0,16	7,98	8,68	8,37	7,28	04	16
0,19	9,08	9,75	9,10	7,92	07	19
0,22	9,85	10,55	9,61	8,36	09	21
0,25	10,82	11,59	10,25	8,92	12	23

Table III.4.c: Numerical comparison of stopping power data [Paul-2013] for ^{63}Cu in ^{63}Cu with Firsov theory and LSS formula.

Also the table III.4.c indicates that the deviation percentages are up to 12 % for the LSS model and up to 23 % for the Firsov's model (same remarks as in Table III.2.a).

Energy MeV/n	S SRIM	S Exp	S LSS	S Fir	Dev/LSS %	Dev/Fir %
Data [Abd-1992-c] Cu on Au (all S units are in MeV.cm².mg^{-1})						
0,43	8,06	7,94	6,64	7,08	16	11
0,71	10,33	10,57	8,53	9,09	19	14
0,80	10,84	9,80	9,05	9,65	08	02
1,02	11,81	11,12	10,22	10,90	08	02
1,13	12,17	12,25	10,76	11,47	12	06

Table III.4.d: Numerical comparison of stopping power data [Paul-2013] for ^{63}Cu in ^{197}Au with Firsov theory and LSS formula.

Table III.4d, indicates that the deviation percentages are up to 19 % for the LSS model and up to 14 % for the Firsov's model.

Energy MeV/n	S SRIM	S Exp	S LSS	S Fir	Dev/LSS %	Dev/Fir %
Data [Pap-1978] Kr on C (all S units are in MeV.cm².mg^{-1})						
0,77	48,63	44,30	39,12	60,46	12	-36
0,65	47,12	45,20	35,93	55,52	21	-23
0,58	45,79	44,40	33,85	52,32	24	-18
0,54	44,98	44,00	32,72	50,57	26	-15
0,41	40,86	38,30	28,48	44,01	26	-15
0,35	38,16	34,90	26,34	40,71	25	-17
0,32	36,28	33,20	25,03	38,68	25	-17

Table III.5.a: Numerical comparison of stopping power data [Paul-2013] for ^{36}Kr in ^{12}C with Firsov theory and LSS formula.

Table III.5.a, indicates that the deviation percentages are up to 26 % for the LSS model and up to 36 % for the Firsov's model.

Energy MeV/n	S SRIM	S Exp	S LSS	S Fir	Dev/LSS %	Dev/Fir %
Data [Gei-1982 & Gei-1983] Kr on Ni (all S units are in MeV.cm².mg^{-1})						
0,51	21,92	20,72	18,03	15,34	13	26
0,88	27,08	25,71	23,62	20,10	08	22
0,92	27,42	26,83	24,16	20,56	10	23
1,28	29,39	29,63	28,56	24,30	04	18

Table III.5.b: Numerical comparison of stopping power data [Paul-2013] for ^{36}Kr in ^{28}Ni with Firsov theory and LSS formula.

Table III.5.b, indicates that the deviation percentages are up to 13 % for the LSS model and up to 26 % for the Firsov's model.

Energy MeV/n	S SRIM	S Exp	S LSS	S Fir	Dev/LSS %	Dev/Fir %
Data [Gei-1982 & Gei-1983] Kr on Au (all S units are in MeV.cm².mg^{-1})						
0,54	10,89	11,21	8,90	8,48	21	24
0,55	10,90	11,07	8,91	8,49	20	23
0,92	13,58	13,22	11,58	11,03	12	17
0,97	13,81	13,83	11,87	11,31	14	18
1,34	15,05	14,71	13,93	13,27	05	10

Table III.5.c: Numerical comparison of stopping power data [Paul-2013] for ^{36}Kr in ^{79}Au with Firsov theory and LSS formula.

Table III.5.c indicates also that the deviation percentages are up to 21 % for the LSS model and up to 24 % for the Firsov's model.

Energy MeV/n	S SRIM	S Exp	S LSS	S Fir	Dev/LSS %	Dev/Fir %
Data [Abd-1992-a] Ag on Al (all S units are in MeV.cm².mg^{-1})						
0,41	32,41	28,47	25,15	28,02	12	02
0,53	36,12	33,60	28,59	31,86	15	05
0,67	39,66	38,31	32,14	35,82	16	07
0,80	42,43	42,57	35,12	39,14	17	08
0,94	45,02	46,15	38,07	42,43	17	08
1,04	46,64	50,10	40,05	44,63	20	11
1,08	47,24	49,89	40,81	45,48	18	09
1,21	49,05	53,36	43,20	48,14	19	10
1,35	50,73	53,03	45,63	50,84	14	04
1,35	50,73	52,25	45,63	50,84	13	03
1,52	52,49	53,82	48,42	53,95	10	00
1,60	53,22	55,92	49,67	55,35	11	01
1,67	53,82	53,74	50,75	56,55	06	-05
1,81	54,85	53,88	52,83	58,87	02	-09

Table III.6.a: Numerical comparison of stopping power data [Paul-2013] for ^{47}Ag in ^{13}Al with Firsov theory and LSS formula.

From table III.6.a we can see that the deviation percentages are up to 20 % for the LSS model and up to 11 % for the Firsov's model.

Energy MeV/n	S SRIM	S Exp	S LSS	S Fir	Dev/LSS %	Dev/Fir %
Data [Rib-1983] Ag on Zn (all S units are in MeV.cm².mg^{-1})						
0,06	3,82	5,71	6,55	5,49	-15	04
0,07	4,98	6,99	7,57	6,34	-08	09
0,09	6,13	8,17	8,46	7,09	-04	13
0,11	7,25	9,28	9,27	7,76	00	16
0,14	8,87	10,85	10,36	8,68	05	20
0,17	10,40	12,33	11,35	9,51	08	23
0,20	11,85	13,73	12,26	10,27	11	25

Table III.6.b: Numerical comparison of stopping power data [Paul-2013] for ^{47}Ag in ^{30}Zn with Firsov theory and LSS formula.

Also from the table III.6.b the deviation percentages are up to 15 % for the LSS model and up to 25 % for the Firsov's model.

Energy MeV/n	S SRIM	S Exp	S LSS	S Fir	Dev/LSS %	Dev/Fir %
Data [Rib-1983] Ag on Pd (all S units are in MeV.cm^2.mg^{-1})						
0,06	3,18	3,52	5,07	4,07	-44	-16
0,07	4,18	4,43	5,85	4,70	-32	-06
0,09	5,26	5,30	6,54	5,26	-23	01
0,11	6,33	6,13	7,17	5,76	-17	06
0,14	7,89	7,33	8,02	6,44	-09	12
0,17	9,35	8,48	8,78	7,05	-04	17
0,20	10,69	9,60	9,48	7,62	01	21
0,22	11,93	10,68	10,14	8,14	05	24

Table III.6.c: Numerical comparison of stopping power data [Paul-2013] for ^{47}Ag in ^{46}Pd with Firsov theory and LSS formula.

The deviation percentages are up to 44 % for the LSS model and up to 24 % for the Firsov's model especially at low energies. We remark high deviations for low velocities.

In conclusion, we can say that in the majority of cases the deviation of the two models does not exceed 20% if we ignore the low velocities deviations (due contribution of nuclear stopping power). The average values of the deviations are relatively large for the lighter and heavier projectiles compared to the intermediate projectiles. Is this due to the fact that the Thomas-Fermi atomic model is much more reliable for relatively high Z, and that heavy projectiles are likely to lose more electrons than intermediate projectiles?

9. The Z oscillations

According to the LSS model and the Firsov model, the rate of energy loss is proportional to the square root of the energy of the projectile, and the stopping powers are monotonic functions of the atomic numbers of the projectiles and targets, however experimental indicates a Z1 and Z2 oscillation of the stopping power for many types of projectiles and targets. Both models violate this experimental phenomenon of Z1 and Z2 oscillation [Den-1977].

In following we study the Z2 oscillation for Mg, Cu and Ag incident ions for fixed value of energy. We consider that the data given by SRIM computation are in agreement with the experimental data.

The graphs data are obtained from the semi empirical SRIM program, which often gives great agreement with experimental data, by fixing the projectile energy and varying the atomic number of the target, to obtain the stopping power as a function of the target Z.

These graphs show clearly the Z2 oscillation phenomenon:

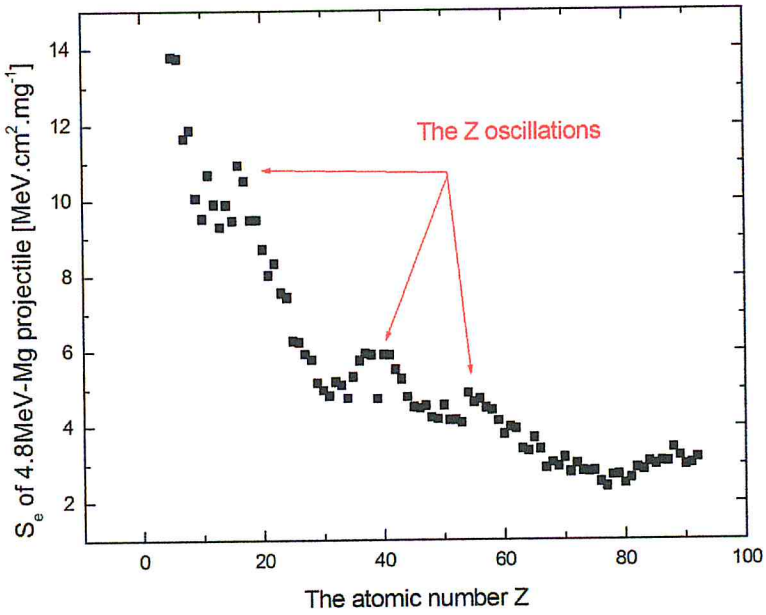

Fig. III.7: Stopping power of 4.8-MeV Mg projectile in targets with various atomic number Z show the Z oscillations.

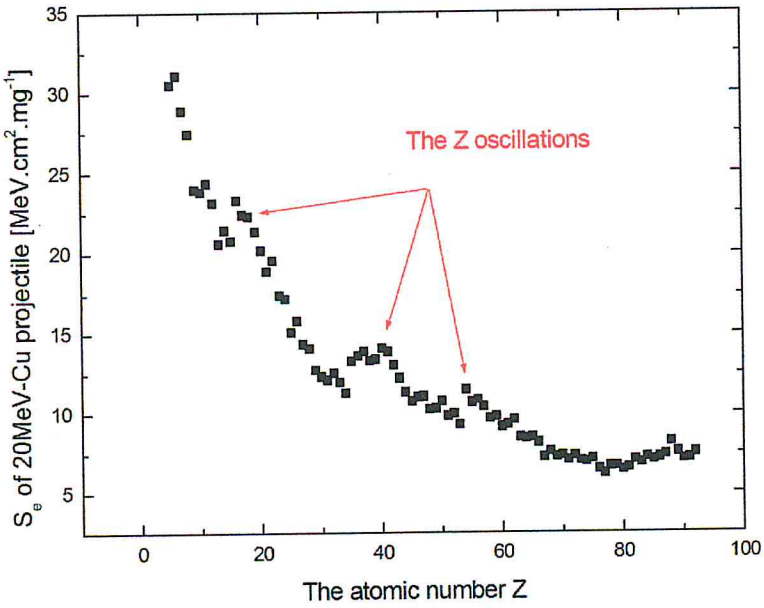

Fig. III.8: Stopping power of 20-MeV Cu projectile in targets with various atomic number Z show the Z oscillations.

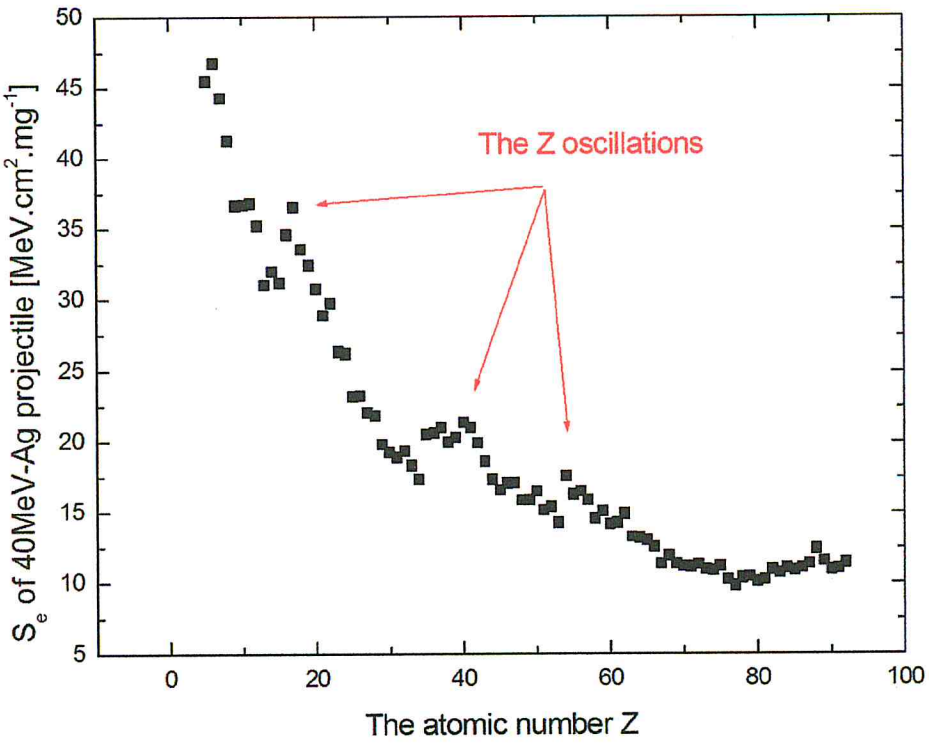

Fig. III.9: Stopping power of 40-MeV Ag projectile in targets with various atomic number Z show the Z oscillations.

So this is one of the shortcomings of the two theories. The Thomas-Fermi atomic model on which the LSS Firsov's models are based is a statistical model, consequently, the atomic shells do not intervene and its effect does not appear in the results of the calculations.

In this chapter, we have presented, compared and discussed by using figures and tables, the results of the stopping powers of some projectiles, obtained by the SRIM program, LSS theory, Firsov's theory and available data, Then we have discussed the Z oscillations which are due to the shell structure of the atoms.

Conclusion

In this work we have presented a comparison between Firsov and the Lindhard-Scharff-Schiott (LSS) stopping power models and experimental data. The stopping power phenomenon results from various physical interaction processes (excitation, ionization…). From the physical point of view of the projectile-target atom interactions, we distinguish two different mechanisms of energy loss: 1) Nuclear stopping power, in which energy is transmitted as translatory motion to a target atom; 2) Electronic stopping power, in which the moving particle loses its kinetic energy by exciting or ejecting atomic electrons. For another classification according to the ion energy we distinguish: 1) The low energies region which contains the LSS (Lindhard, Sharff and Schiott) domain of energies where the stopping power is approximately proportional to the ion velocity i.e. the square root of the ion energy, this region is the interesting region of this work, 2) the intermediate region, and 3) the Bethe-Bloch region for high energies of ions.

Many reasons lead to the need of looking for an accurate theoretical expression of stopping power. First of all, the stopping power represents an indispensable and critical quantity in several fields of technology (such as ion beam analysis, ion implantation, radiation therapy…). Also, large deficiencies and discrepancies appear in available data. Moreover, performing experiments to determine the stopping power of a projectile at a well-defined energy using thin films is very expensive.

In 1957 Firsov obtains an interatomic potential for statistical Thomas-Fermi atoms. By assuming that the transfer of electrons between the projectile and target atoms is the mechanism for energy loss, Firsov obtains in 1959 an expression for the energy loss in a single collision at low-velocity region $v \leq v_0 Z_1^{2/3}$ (LSS region).

The Lindhard-Scharff-Schiott model (LSS model) is also based on Thomas-Fermi atomic model, it offers analytical formula the electronic stopping power of particles through matter as the Firsov's model in the low-velocity region (LSS region).

For the comparison between the two models, both the Firsov and LSS formulas are proportional to the ion velocity i.e. the square root of the ion energy. The choice of interatomic potential is different. The Firsov's model assumes neutral collision partners and ignores ionization. The stopping power reciprocity (i.e. $S(Z_1\ in\ Z_2) = S(Z_2\ in\ Z_1)$) is verified in the Firsov's model but not in the LSS model.

From the comparison between the two theoretical models and experimental data in the chapter III, we can say that in the majority of cases the deviation of the two models does not exceed 20% if we ignore the low velocities deviations (due contribution of nuclear stopping power).

The Z oscillations phenomenon is one of the shortcomings of the two theories. The Thomas-Fermi atomic model on which the LSS Firsov's models are based is a statistical

model, consequently, the atomic shells do not intervene and its effect does not appear in the results of the calculations.

Although the theoretical results of the Firsov and LSS models are somewhat similar to the experimental data, the work in the field remains insufficient and much more effort is required in order to get more reliable theoretical expression for the stopping power.

References

[Abd-1992-a] M. Abdesselam, J.P. Stoquert, G. Guillaume, M. Hage-Ali, J,J. Grob and P. Siffert, Nuclear Instruments and Methods in Physics Research B72 (1992) 293-301

[Abd-1992-c] M. Abdesselam, J.P. Stoquert, G. Guillaume, M. Hage-Ali, J.J. Grob and P. Siffert, Nuclear Instruments and Methods in Physics Research 872 (1992) 7-15

[All-1996] A. Allisy, Volume 68, Issue 1-2, 1 November 1996, Pages 3–10

[Ars-1990] K. Arstila, J. Keinonen, and P. Tikkanen, Physical Review B Volume 41, Number 10 (1990)

[Boh-1954] N. Bohr and J. Lindhard, Dan. Mat. Fys. Medd. 28, No. 7 (1954)

[Boo-65] W. Booth and I. S. Grant, Nuclear Physics. 63,481, 1965

[Den1977] N. M. Denkin, Stopping Power of Gases for Heavy Ions, California Institute of Technology (Thesis), 1977

[Fas-1966] B. Fastrup, P. Hvelplund and C. A. Sautter, K. Dansk. Videnskab. Selskab, Mat.-Fys. Medd. 35 no. 10

[Fir-1958-a] O. B. Firsov, Soviet Physics JETP, Vol. 6 (33), No. 3 (1958)

[Fir-1958-b] O. B. Firsov, Soviet Physics JETP Vol. 34 (7), No. 2 (1958)

[Fir-1959] O. B. Firsov, Soviet Physics JETP Vol. 36 (9), No. 5 (1959)

[Gal-1990] A.Galindo, P. Pascual, Quantum mechanics II, Springer-Verlag New York Berlin Heidelberg, (1990)

[Gei-1982] H. Geissel, Y. Laichter, W.F.W. Schneider and P. Armbruster, Phys. Lett. 88a,26, (1982)

[Gei-1983] H. Geissel, Y. Laichter, R. Albrecht, T. Kitahara, J. Klabunde, P. Strehl and P. Armbruster, Nuclear Instruments and Methods 206 (1983) 609-612

[Gue-2014] A.Guesmia, H.Ammi, M.Msimanga, A.Dibb, S.Mammeri, C.A.Pineda-Vargas, M. Hedibel, Radiat. Phys. Chem. 96(2014)205–210.

[Gue-2015] A.Guesmia, H.Ammi, M.Msimanga, A.Dibb, S.Mammeri, C.A.Pineda-Vargas, M. Hedibel, Radiat. Phys. Chem. 107(2015)189-194

[Gue-2016] A. Guesmia, Chapter III, course of an introduction to the slowing down theory

[Gue-2016] A. Guesmia, M. Msimanga, C.A. Pineda-Vargas, H. Ammi, A. Dib, S. Mammeri, Nucl. Instr. and Meth. B 371 (2016) 69–75

[Hab-2011] A. N. Habte, Calculations of Stopping Power and Range of Alpha Particles of Several Energies in Different Materials, Thesis (2011)

[Hil-1989] D. Hilscher, Paramana, Vol. 33, No. 1 (1989)

[Jok-1997] J. Jokinen, Nuclear Instruments and Methods in Physics Research B 124 (1997) 447-452

[Kor-2006] S. Korostiy, Spectroscopic Investigation of the Charge Dynamics of Heavy Ions Penetrating Solid and Gaseous Targets, Thesis (2006)

[Lan-1996] B. Langenbeck, G. Breitenberger, H. Gaiser, F. Klos, G. Moritz and K. Zweig, IEEE Transactions on Magnetics, Vol. 32. No. 4, JULY 1996

[Lin-1963] J. Lindhard, M. Scharff and H. E. Schiott, Mat. Fys. Medd. Dan. Vid. Selsk. 33, No. 14 (1963)

[Mer-1961] E. Merzbacher, Quantum Mechanics, Wiley; 1st edition (1961)

[Msi-2009] M. Msimanga, C.M. Comrie, C.A. Pineda-Vargas, S. Murray, R. Bark, G. Dollinger, Nucl. Instr. and Meth. B 267 (2009) 2671–2674

[Msi-2014] M.Msimanga, C.A. Pineda-Vargas, T. Hlatshwayo, C.M. Comrie, H.Ammi, M. Nkosi, Nucl. Instr. and Meth. B 322 (2014) 54-58

[Nas-1996] M. Nastasi, J. W. Mayer and J. K. Hirvonen, Ion-Solide Interactions: Fundamentals and Applications, Cambridge University Press; 1 edition (March 29, 1996)

[Nas-2015] M. Nastasi, W. Mayer, Y. Wang, Ion Beam Analysis: Fundamentals and Applications, CRC Press Taylor & Francis Group Boca Raton London New York, (2015)

[Pap-1978] H. Pape H. G. Clerc K. H. Schmidt, Z.f. Physik A286,159, 1978

[Paul-2013]: H. Paul, Stopping power for heavy, http://www.exphys.uni-linz.ac.at/stopping/

[Rib-1983] R. V. Ribas, W. A. Seale, and M. N. Rao, Phys. Rev. A28, 3234, 1983

[Shu-2015] A. Shukri, Ab Initio Electronic Stopping Power In Materials, Thesis (2015).

[Sig-1983] P. Sigmund, Physica Scripta. Vol. 28,257-267 (1983)

[Sig-2000] P. Sigmund, Stopping Power: Wrong Terminology, ICRU News (2000)

[Sig-2004] P. Sigmund, Stopping of Heavy Ions: A Theoretical Approach, Springer-Verlag Berlin and Heidelberg (2004)

[Sig-2006] P. Sigmund, Particle Penetration and Radiation Effects, Springer Berlin Heidelberg New York (2006)

[Sig-2008] P. Sigmund, Springer, Volume 72, Issue 5, pp 569-578 (2008)

[Ter-2007] Terry L. Alford, Leonard C. Feldman and James W. Mayer, Fundamentals of Nanoscale Film Analysis, Springer (2007)

[Zha-2002] Y. Zhang, Nuclear Instruments and Methods in Physics Research B 196 (2002) 1–15

[Zie-2008] J. F. Ziegler, J. P. Biersack, M. D. Ziegler; SRIM The Stopping and Range of Ions in Matter (2008)

[Zie-2013] J. F. Ziegler, The stopping and Range of Ion in Matter (http://www.srim.org/, version 2013)